ENERGY, ENVIRONMENT
&
STORAGE

AN INTERNATIONAL JOURNAL

Volume-2
Issue-1
January, 2022
ISSN:2791-6197

Editor in Chief
Dr. Selahaddin Orhan AKANSU

HYDROGEN ROMANTIC

by Anna Green

About the Book

The idea of the Hydrogen Romantic book came to my mind after working for several years with the leading hydrogen energy scientists and observing their activities. One of those scientists, Dr. Turhan Nejat Veziroglu, has devoted his life to this topic, becoming much loved and respected around the world. In addition to all the momentous events in which Dr. Veziroglu has been involved, his memories are very interesting. Such a life is almost like navigating the pages of history, allowing admirers to gain information without being bored. I asked him to spend one hour with me every day, so I could interview him. During those one-hour periods, I asked him questions, and I recorded his responses. After I finished the interviews, I listened to the recordings. From this, I wrote the book. In addition, I did research on the sections dealing with the historical events. I've added this research as narratives in the book.

Book Details

Language : English

Publication Date : 12/29/2020

Format : Softcover

Dimensions : 6x9

Page Count : 286

ISBN : 9781664126992

Format : Hardcover

Softcover	Hardcover	E-Book
$17.99	$31.99	$3.99

https://www.xlibris.com/en/bookstore/bookdetails/759083-hydrogen-romantic

ENERGY, ENVIRONMENT AND STORAGE

EES JOURNAL

Founded and Published by Erciyes Energy Association

Energy, Environment and Storage Journal is indexed in Crossref

Printed in Turkey

ISSN-2791-6197

EES- EDITORIAL BOARD

BOARD MEMBERS:

AIM AND SCOPE

Energy, Environment and Storage papers consider the prospects of energy technologies, environment, materials, process control and industrial systems. The Energy, Environment and Storage will be published 3 times per year.

Contributions describe novel and significant applications to the fields of:

- Hydrogen Fuels
- Hydrogen and Fuel Cell
- Hydrogen Economic
- Biomass
- Solar PV Technology
- Solar Thermal Applications
- Wind Energy
- Materials for Energy
- Drones and Energy Applications
- Nuclear Energy and Applications
- Hydro Power
- Fuel Technologies (CNG, LNG, LPG, Diesel, Gasoline, Ethanol, etc.)
- Numerical Modelling
- Energy Storage and Systems
- Battery Technologies
- Energy Management
- Heat and Mass Transfer
- Aerodynamics
- Aerospace and Energy Applications
- Combustion
- Electric Vehicle Transportation
- Off-grid Energy Systems
- Environment Management
- Air Pollution
- Water and Wastewater Pollution
- Water and Wastewater Management
- Waste Management
- Global Warming and Climate Change
- Environmental Ecosystem
- Environmental System Modelling and Optimization
- Ecological Applications or Conservation

CONTENTS

Research Article *Energy, Environment and Storage* (2022) 02-01:1-10

Energy, Environment and Storage

JournalHomepage: www.enenstrg.com

A Novel Fully Controllable Rotary Switch for Electrical Installation in Buildings

Claude Ziad El-Bayeh[1*], Mohamed Zellagui[2], Brahim Brahmi[3]

[1]*Canada Excellence Research Chair Team, Concordia University, Canada, ORCID: 0000-0002-8268-8878*

[2]*Department of Electrical Engineering, Faculty of Technology, University of Batna 2, Fesdis, 05078, Batna, Algeria, ORCID: 0000-0003-2558-2273*

[3]*Electrical and Computer Engineering Department, Miami University, Oxford, USA, ORCID: 0000-0002-4486-0710*

ABSTRACT. In an electrical installation in buildings, electromechanical switches are mostly used to turn on and off a load. However, sometimes there are two or more switches in the same circuit intended to control the same load. Thus, a conflict can happen between multi-users who are trying to overtake the control of the load (such as turning it on or off). To solve the problem, this paper proposes a novel switch called "Fully Controllable Rotary Switch" (FCRS) in which it can fully control not only the load but also other switches by blocking them or giving them limited or full access over the electrical circuit and the loads. For validation purposes, the utilization of FCRS in buildings is compared to the traditional switches under the same functionality and conditions. Results show that FCRS has the ability to control many electrical loads simultaneously, control other switches in the circuit, increase the satisfaction, security, and privacy of the users. Finally, it reduces the conflict between multi-users and the investment cost by avoiding installing additional switches and protection devices.

Keywords: Rotary switch, Switch, Buildings, Electrical installation, Control loads.

Article History: Received:16.08.2021; Revised:26.09.2021; Accepted:02.10.2021; Available online: 13.10.2021
Doi: https://doi.org/10.52924/DKMA3371

NOMENCLATURE

1P1T	Single pole, Single Throw Switch
1P2T	Single pole, Double Throw Switch
1PNT	Single pole, N-Throw
2P1T	Double Pole Single Throw Switch
2P2T-R	Double pole, double throw with reverse polarity
DPDT	Double Pole Double Throw Switch
DPST	Double Pole Single Throw Switch
MPNT	M pole, N throw
SPDT	Single Pole Double Throw Switch
SPST	Single Pole Single Throw Switch

1. INTRODUCTION

1.1 Background and motivation

In electrical engineering, a switch is a component that is able to turn on and off one or more electrical elements, connect or disconnect the conducting path in an electrical circuit, divert the electric current from one conductor (or wire) to another, and interrupt the electric current flow in a conductor [1, 2]. Electromechanical device switches are considered the most common switches, which consist of one or more sets of movable electrical contacts connected to external circuits [3, 4]. When the pair of contacts in the switch are touching (also called closed contact), the current flows in the circuit, and the electrical elements are turned on. When the contacts are separated (also called open contacts), the current cannot flow, and the electrical elements are turned off [4, 5].

Different configurations exist for the switches. Switches may have many sets of contacts controlled by the same actuator or knob, and the contacts can operate alternately, sequentially, or simultaneously [6]. Switches can operate manually (e.g., light switch), or using a sensing element (e.g., temperature sensor, motion sensor, etc.) [6]. There are many existing forms of switches such as circuit breakers, relays, reversing switches, push-button switches, mercury switches, rotary switches, and toggle switches [7-9]. Despite the different forms of switches, they function in the same way in which they open or close electrical contacts to control the current flow in conductors. Usually, each contact is connected to only one conductor. Hence, the question that arises, what happens if one electrical contact in the switch can be connected to two or more other terminal contacts instead of just one? Will it give

*Corresponding author: c.bayeh@hotmail.com

more controllability to the user and increase security? Will it facilitate the daily usage of electricity, especially in buildings? What if many users have access to control a certain load simultaneously, which of them will have more privilege than others to control the load? To the best of the author's knowledge, the existing switches cannot answer these questions and cannot meet the requirements of certain users. Hence, a new type of switches should be designed to answer all these questions.

1.2 Literature review

In the field of electrical installation in buildings, switches play an important role in controlling electrical elements by turning them on or off, such as light bulbs, fans, air conditioners, water heaters, and many others [10, 11]. The most familiar form of switches is manual-based mechanical devices with one or more sets of electrical contacts connected to external circuits. A set of contacts is composed of two contacts that can be either connected or not connected. If they are connected, the current flows in the circuit, and we call it "closed". In case they are not connected, we call it "open" since the current cannot flow in the circuit. Fig. 1 presents the difference between closed and open contacts.

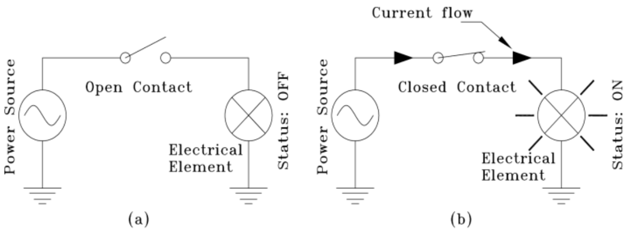

Fig. 1. Open and closed contacts of a switch.

A switch can have many poles and throws. The number of poles is the number of an electrically separate set of contacts that are controlled by a single physical actuator. Fig. 2 shows examples of different forms of switches with a different number of poles. The one-pole switch can be used for a single-phase circuit in which it can only connect or disconnect a phase. A double-pole switch has two separate parallel sets of contacts, which open and close simultaneously via the same mechanism. This can be used to separate the phase and neutral in a single-phase circuit, or 2 phases in a two-phase circuit, etc., [12-14].

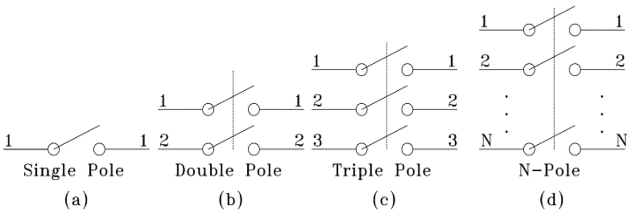

Fig. 2. Different number of poles in a switch.

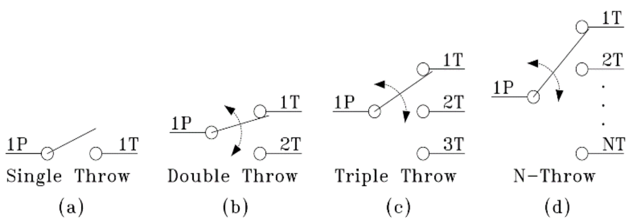

Fig. 3. Different number of throws in a switch.

The number of throws presents the number of available paths for each pole in which the switch can adopt [12-14]. Fig. 3 shows different number of throws in a switch. If a switch has only one throw, it can only control one circuit. If a switch has two throws, it can maximum control two circuits, and the current can flow either in the first or in the second circuit and not both simultaneously.

Table 1. Most common switches.

Abb.	Name	Description	Symbol
SPST 1P1T	Single pole, single throw	A simple on-off switch. The two terminals are either connected or disconnected. If the two terminals are normally disconnected, the switch is called Normally Open (1P1T-NO). If the two terminals are normally connected, the switch is called Normally Closed (1P1T-NC), [15-17].	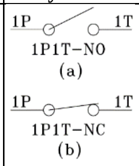
SPDT 1P2T	Single pole, double throw	Two possible switches can be in this case. (a) 1P2T in which the 1P terminal is either connected to 1T or to 2T. (b) 1P2T-CO has an additional center-off position (CO) in which 1P terminal can rest, and it is not connected to any other terminals (1T nor 2T). So, the possible positions, in this case, are, CO, 1T, and 2T, [15-17].	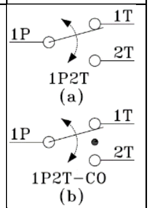
1PNT	Single pole, N-Throw	Two possible switches can be in this case. (a) 1PNT in which the 1P terminal is connected to one of the throw terminals, 1T, 2T, …, or NT. (b) 1PNT-CO has a center off position (CO) in which 1P terminal can rest and it is not connected to any other terminals (1T, to NT). The possible positions in this case are CO, 1T, 2T, …, NT.	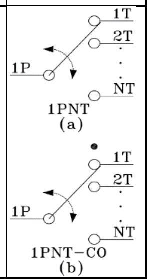
DPST 2P1T	Double pole, single throw	Equivalent to two parallel 1P1T switches controlled by a single mechanism. There are two possibilities. (a) 2P1T-NO, in which a set of contacts is in the initial position normally open (NO). (b) 2P1T-NC in which a set of contacts is in the initial position normally closed (NC), [15-17].	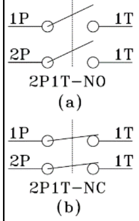
MPNT	M pole, N throw	Equivalent to M parallel 1PNT switches controlled by a single mechanism. There are two possibilities. (a) MPNT, in which the first terminal (1P, 2P, …) is connected to one of the existing N terminals (1T, 2T, …, NT). (b) MPNT-CO, in which the first terminal (1P, 2P, …) can have a rest position and may not be connected to any of the N terminals (1T, 2T, …, NT).	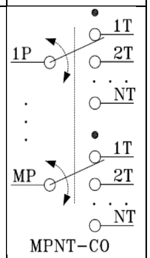
2P2T-R	Double pole, double throw with reverse polarity	The switch is able to reverse polarity by changing its position. The first position, 1P terminal is connected to 1T, and 2P is connected to 2T. Once the switch is pressed, the polarity is changed and 1P terminal becomes connected to 2T, and 2P becomes connected to 1T, [15-17].	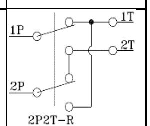

The number of throws presents the number of available paths for each pole in which the switch can adopt [12-14]. Fig. 3 shows different number of throws in a switch. If a switch has only one throw, it can only control one circuit. If a switch has two throws, it can maximum control two circuits, and the current can flow either in the first or in the second circuit and not both simultaneously.

Table 1 shows the most common switches used in electrical installation in buildings. For lighting, 1P1T (one-pole, one-throw), 1P2T (one-pole, two-throw), and 2P2T-R (polarity-reversal two-pole, two-throw) are mostly used.

Table 2. Other type of switches Part I.

Name	**Description**	**Picture / Symbol**
Centrifugal switch	It operates using the centrifugal force resulting from a rotating shaft (e.g., electric motor,and gasoline engine). It is designed to activate or de-activate as a function of the rotational speed of the shaft[18].	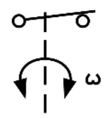
Company switch	Itis used for power distribution systems in convention centers, arenas, theaters, etc.,that often require panel boards for electrical equipment. It is designed to be easy to use, easily portable, safe and fast[19].	
Dead man's switch	It is a switch designed to be activated or deactivated if the human operator becomes incapacitated (i.e., through death, loss of consciousness, or being bodily removed from control). It can be applied to switch on/off vehicle, machine, computer, etc.[20].	
Fireman's switch	It allows firefighters to quickly disconnect power from high voltage devices that may cause a danger inemergencycases [21].	
Hall effect sensor	It is a type of sensor which detects the presence and magnitude of a magnetic field using the Hall effect[22]. It is used for proximity sensing, positioning, speed detection, and current sensing applications. Usually, it is combined with threshold detection to act as a binary switch. Hall effect sensors are used in industrial applications and in consumer equipment (i.e., detecting missing papers in some computer printers).	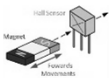
Inertial switch	It is an electrical switch which is firmly mounted upon some equipment such as a vehicle or other mobile device, that triggers in the event of shock or vibration[23, 24]. Once it is triggered, it may either enable or disable some functions such as stopping the fuel pump during a car collision or accident in order to avoid fire hazard.	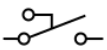
Isolator switch	It is used to ensure that an electrical circuit is completely disconnected for service or maintenance [25].	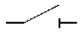
Key switch	It is a key-operated switch.It is used in situations where access needs to be restricted to the switch's functions such as lunching nuclear missiles [26, 27].	
Emergency switch	It is a safety mechanism used to shut off machinery in an emergency, when it cannot be shut down in the usual manner.	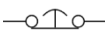
Latching switch	A latching switch is a switch that maintains its state after being activated.[1] A push-to-make, push-to-break switch would therefore be a latching switch – each time you actuate it, whichever state the switch is left in will persist until the switch is actuated again[28].	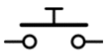
Light switch	It is used to turn on/off electric lights, permanently connected equipment, or electrical outlets. Different types exist including: (a) and remotely controlled switches and dimmers; (b) occupancy-sensing switches; (c) time-controlled switches; (d) dimmer switches that allow controlling the brightness of lamps as well as turning them on or off; and (e) light switch mounted on the socket, base, or in-line with the cord.	
Pull switch	It is actuated by means of a chain or string. Once the string is pulled, one pull is to switch on and next pull is to switch off. Mostly used to turn on/off ceiling lights and fans[29].	

1.3 Other types of switches

There are other types of switches that can have different functionalities. **Table 2** and **Error! Not a valid bookmark self-reference.**show the 20 most used switches in engineering. In addition, we classify the switches into many categories as depicted in **Fig.4**.

Table 3. Other type of switches Part II.

Name	**Description**	**Picture / Symbol**
Membrane switch	It is an electrical switch for turning on/off a circuit. It is a circuit printed on Polyethylene terephthalate or Indium tin oxide in which it is mostly used as user-equipment interface utilities that allow for the communication of commands from users to electronic devices such as printer, keyboard, etc., [30].	
Optical switch	It amplifies weak optical signals from the input. Light occurring on an optical transistor's input changes the intensity of light emitted from the transistor's output while output power is supplied by an additional optical source. It is mostly used in optical computing and fiber-optic networks[31].	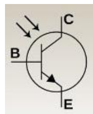
Piezo switch	It generates electric charge when certain materials are under stress or pressure. It works using Piezoelectric effect. The stress could be a force from compressive pressure that causes the piezo element to bend very slightly like a drumhead and be activated.	
Push button switch	It is a momentary or non-latching switch which causes a temporary change in the state of an electrical circuit only while the switch is physically actuated. An automatic mechanism (i.e. a spring) returns the switch to its default position immediately afterwards, restoring the initial circuit condition [32].	
Stepping switch	It is an electromechanical device that switches an input signal path to one of several possible output paths, directed by a train of electrical pulses[33].	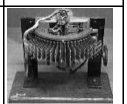
Time switch	It is a timer that operates an electric switch controlled by the timing mechanism (could be mechanical or electronic). It has several applications, as an example, a sleep timer is a function on many modern televisions and other electronic devices that shuts off the power after a preset amount of time[34].	
Touch switch	It is a type of switch that only has to be touched by an object to operate. It is used in many lamps and wall switches that have a metal exterior as well as on public computer terminals. A touchscreen includes an array of touch switches on a display. A touch switch is the simplest kind of tactile sensor.	
Transfer switch	It switches a load between two sources. It can be manual (by throwing a switch), or automatic (when it senses one of the sources has lost or gained power). As an example, an Automatic Transfer Switch (ATS) is often installed where a backup generator is located, so that the generator may provide temporary electrical power if the utility source fails[35].	

1.3 Contribution

The main problem of the existing architecture of the switches is that they are not able to connect more than one circuit at a time (e.g., 1P terminal cannot be connected to 1T and 2T terminals simultaneously in the switch 1P2T). In addition, they do not give the user a full control of all circuits especially when more than one switch is located on the same circuit. Therefore, an original switch should be developed in order to increase the controllability of many circuits at the same time. For this purpose, a novel switch called Fully Controllable Rotary Switch (FCRS) is designed in this paper, in which it increases the controllability over many circuits simultaneously, increase privacy and security, and reduce the investment cost. For validation purposes, the novel switch is compared to existing switches that are used to control electrical loads in buildings.

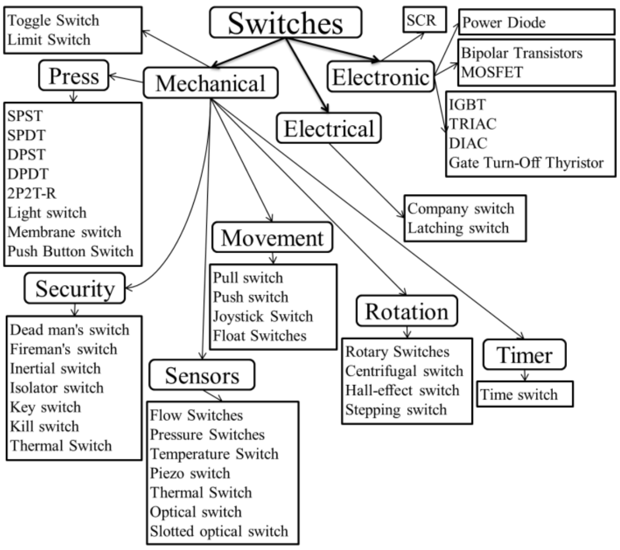

Fig.4. Classification of switches.

2. DESIGN OF A FULLY CONTROLLABLE ROTARY SWITCH

2.1 Mathematical background

The number of terminals and contacts of the Fully Controllable Rotary Switch (FCRS) depends on how many circuits we would like to control and what is the main use of it. Generally speaking, if M and N represent the number of poles and throws of the switch, respectively, the number of possible positions (P) for the contacts in the FCRS is presented in Eq. (1). As an example, if the switch has the form of 1P2T, 3 terminals exist (including the pole terminal), and the total number of possible positions is equal to $2^{(3-1)} = 4$. If the switch has the form of 1P3T, the total number of possible positions or combinations is equal to $2^{(4-1)} = 8$.

$$P = M2^{(T-1)} \tag{1}$$

The rotation angle that should separate the terminals in the switch is described in Eq. (2) and presented in Fig. 5.

$$\theta = \frac{360^o}{2^{(T-1)}} \tag{2}$$

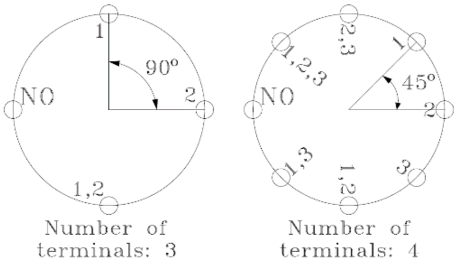

Fig. 5. Rotation angle separating the terminals.

The maximum number of connections (n) between positions is determined by Eq. (3). Where, P is the number of possible positions.

$$n = \frac{P(P-1)}{2} = \frac{M2^{(T-1)}\left(M2^{(T-1)}-1\right)}{2} \tag{3}$$

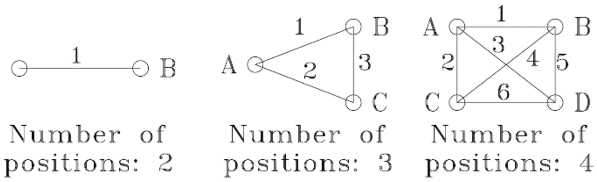

Fig. 6. Number of connections as a function of the number of positions.

The maximum number of configurations C is determined by Eq. (4) and Eq. (5), where C is a function of the number of terminals.

$$C = \sum_{i=0}^{n} \frac{(n)!}{i!\,(n-i)!} \tag{4}$$

$$C = \sum_{i=0}^{\frac{M2^{(T-1)}\left(M2^{(T-1)}-1\right)}{2}} \frac{\left(\frac{M2^{(T-1)}\left(M2^{(T-1)}-1\right)}{2}\right)!}{i!\left(\frac{M2^{(T-1)}\left(M2^{(T-1)}-1\right)}{2}-i\right)!} \tag{5}$$

Table 4. Number of connections as a function of the number of the possible positions.

Number of positions P	Maximum number of connections n	Shape of the switch	θ	maximum number of configurations
2	1	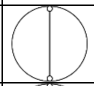	180	2
3	3	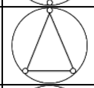	120	8
4	6	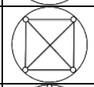	90	64
5	10	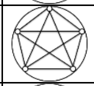	72	1,024
6	15	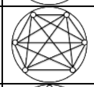	60	32,768
7	21	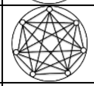	41.428	2,097,152
P	$\frac{\mathrm{P(P-1)}}{2}$		$\frac{360^o\mathrm{M}}{\mathrm{P}}$	$\sum_{\mathrm{i=0}}^{\frac{\mathrm{P(P-1)}}{2}} \frac{\left(\frac{\mathrm{P(P-1)}}{2}\right)!}{\mathrm{i!}\left(\frac{\mathrm{P(P-1)}}{2}-\mathrm{i}\right)!}$

2.2 Design of a Fully Controllable Rotary Switch

In this section, the design of a Fully Controllable Rotary Switch (FCRS) is presented, in which only three types are shown FCRS-1P2T, FCRS-1P3T, and FCRS-2P3T. Fig.7 presents the design of a FCRS of the type 1P2T (one-pole, two-throw). Internal connections and the external look of the switch are presented in the figure. There are 4 possible connections in this switch, (a) the switch is off, (b) terminal 1P is connected to terminal 1T, (c) terminal 1P is connected to terminal 2T, (d) terminal 1P is connected to both terminals 1T and 2T. Therefore, the switch gives the user full control over the two circuits (connected to 1T and 2T), which is not the case with any traditional switch. By adding internal barriers (in Fig.7 barriers a, b, c, and d), it is possible to limit the rotation of the switch and forbid it to reach a certain position. For example, if barrier “a” and “c” are activated, the switch cannot reach the position “NO” normally open. Hence, the only states can be:

1) terminal 1P is connected to terminal 1T,
2) terminal 1P is connected to terminal 2T
3) terminal 1P is connected to both terminals 1T and 2T

In case the barriers “c” and “d” are activated, the switch cannot reach the position “1,2”, and the only states can be as follows:

1) the switch is off,
2) terminal 1P is connected to terminal 1T,
3) terminal 1P is connected to terminal 2T

From this place, adding internal barriers can increase the complexity of the switch and give it much more control over all circuits.

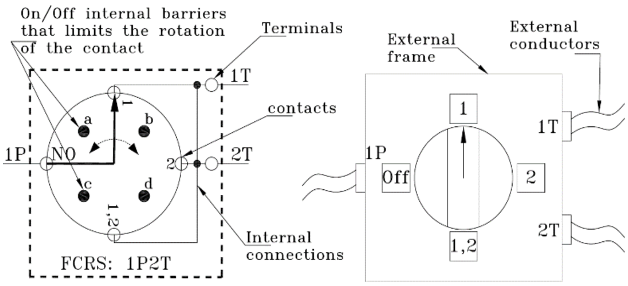

Fig.7. Internal and external design of FCRS-1P2T.

Fig.8 presents the design of a FCRS of the type 1P3T (one-pole, three-throw). Internal connection and external look of the switch are presented in the figure. There are 8 possible connections in this switch as follows:

1) the switch is off,
2) terminal 1P is connected to terminal 1T,
3) terminal 1P is connected to terminal 2T
4) terminal 1P is connected to terminal 3T
5) terminal 1P is connected to both terminals 1T and 2T
6) terminal 1P is connected to both terminals 1T and 3T
7) terminal 1P is connected to both terminals 2T and 3T
8) terminal 1P is connected to all terminals 1T, 2T and 3T

The switch gives the user a full control over the three circuits (connected to 1T, 2T, and 3T) which is not the case of any traditional switch.

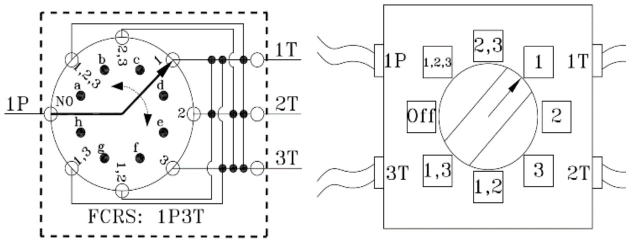

Fig.8. Internal and external design of FCRS-1P3T.

Fig.9 presents the design of an FCRS of the type 2P3T (two-pole, three-throw). Internal connection and external look of the switch are presented in the figure. Similar to the previously mentioned switch 1P3T, there are 8 possible connections for each pole in this switch. Hence, the total number of possible connections is 16 for all poles. The contacts of all poles can be rotated by a single or separate axis. In the case of a single rotating axis, all poles in the switch will be connected to the same terminal positions. In another meaning, if 1P is connected to 2T in the first layer, then 2P will also be connected to 2T in the second layer. However, for a multi-rotating axis, each pole is controlled by its own rotating mechanism and the contact position may not be the same for different poles. In another meaning, if 1P is connected to 2T in the first layer, 2P could be connected to 3T or any other terminal. Hence, this kind of switches gives a full control over all circuits connected to the switch, which is the main originality of this work. With the same analogy, any FCRS-NPMT can be created with “N” Poles and “M” Throws.

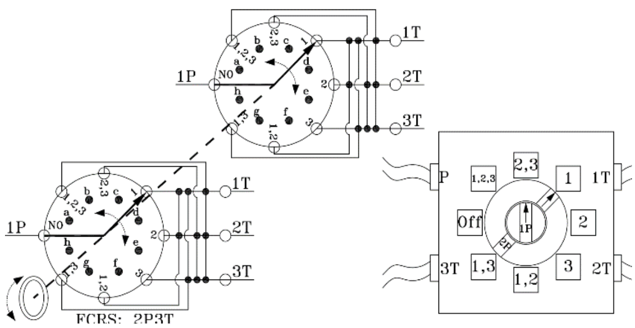

Fig.9. Internal and external design of FCRS-2P3T.

3. APPLICATION OF THE FULLY CONTROLLABLE ROTARY SWITCH IN ELECTRICAL INSTALLATION IN BUILDINGS

In this section, only FCRS-1P2T and 1P3T are chosen and compared to the traditional 1P1T, 1P2T, and 2P2T-R switches in the field of electrical installation in buildings. The main goal is to give the user a full controllability over the electrical elements (such as lighting, machines, etc.), especially when there are multi-users who can also control the same element.

3.1 1P1T Switch vs FCRS-1P2T

FCRS-1P2T can be used to replace the 1P1T switch and it can control the electrical load in the same way as presented in Fig.10. The load is branched to 1T contact in the FCRS. Hence, to turn on the load, it is sufficient to rotate the switch to any position that has the number “1”, (such as: “1” and “1,2”). To turn it off, it is sufficient to rotate the switch to any other position (such as” “Off”, and “2”).

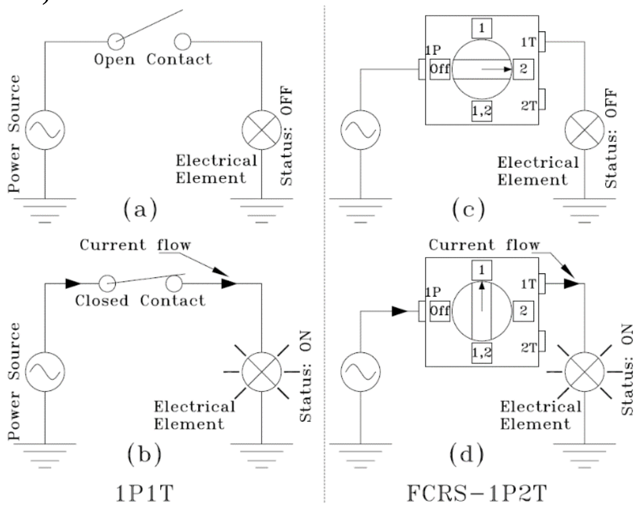

Fig.10. 1P1T Switch vs FCRS-1P2T.

3.2 1P2T Switch vs FCRS-1P2T

Similar to the previous subsection, FCRS-1P2T can replace 1P2T switch as presented in **Fig. 11**. 1P2T switch can either turn on load 1 or load 2. FCRS-1P2T has an advantage over 1P2T switch in which it has more states, such as turning off all loads, turning on load 1, turning on load 2, and turning on load 1 and 2 simultaneously as in**Fig. 11**.

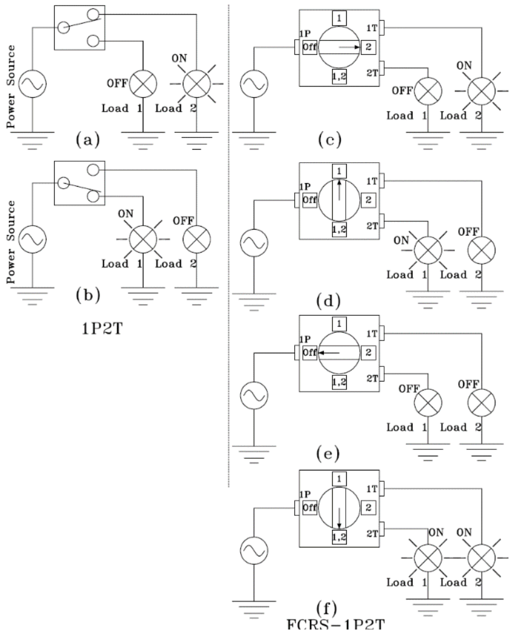

Fig. 11. Example 1, 1P2T Switch vs FCRS-1P2T.

3.3 Two 1P2T switches vs. two FCRS-1P2T

Suppose that two switches are used to control a light bulb in a room as in Fig. **12**. Each switch is located next to a door, one on the entrance and one on the exit. The light can be controlled by any switch and has one of the two states, either on or off.

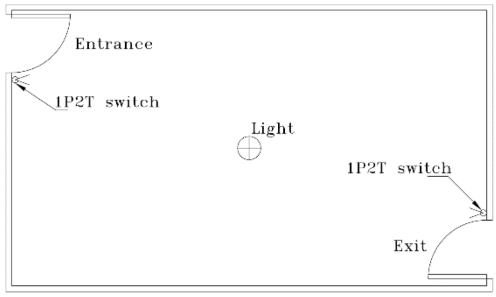

Fig. 12. Controlling light in a room using two 1P2T switches vs. two FCRS-1P2T.

Fig.13 and Table 5 present all possible contact positions for the two switches. It can be remarked that the light is turned on only if both switches are in the same contact positions.

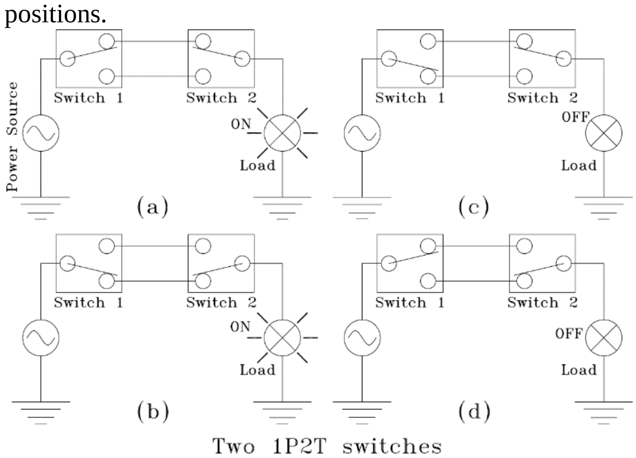

Fig.13. All possible contact positions for both switches of type 1P2T.

Table 5. Possible combination of contact positions of two 1P2T switches.

		Switch 1	
		Position 1	Position 2
Switch 2	Position 1	On	Off
	Position 2	Off	On

For the case of using the proposed FCRS-1P2T, there are lots of ways to control the light, which also depends on the connection type of the terminals of the switch and the configuration of the switches. The control can be divided into six main categories as follows:

- Switch 1 has full control of the load disregarding the contact positions in switch 2, (refer to configuration 1 in Fig.14 and Table 6),
- Switch 2 has full control of the load disregarding the contact positions in switch 1, (refer to configuration 2 in Fig.14 and Table 7),
- Switch 1 and 2 can equally control the load without any preference to any switch, (refer to configuration 3 in Fig.14 and Table 8),
- Switch 1 and 2 can control the load with a slight preference to switch 1, (refer to configuration 4 in Fig.14 and Table 9),
- Switch 1 and 2 can control the load with a slight preference to switch 2, (refer to configuration 5 in Fig.14 and Table 10),
- Other configurations (refer to configuration 6 in Fig.14 and Table 10),

The possible configurations are not limited to the ones presented in Fig.14. There are many other ways to configure the connection; however, only six selected configurations are presented in this section. FCRS allows us to make a large number of different configurations, in which each one operates in a different way according to the needs of the users. Hence, using the proposed FCRS gives much more flexibility to control the loads compared to the traditional switches such as 1P2T.

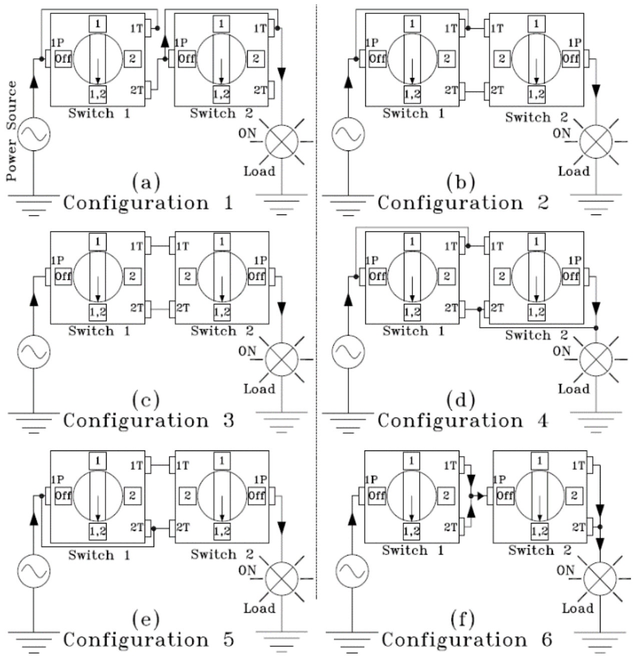

Fig.14. Six selected configurations of connecting two FCRS-1P2T switches.

Table 6. Possible combination of contact positions of the two FCRS-1P2T switches for configuration 1.

		Switch 1			
		Off	1	2	1,2
Switch 2	Off	Off	Off	On	On
	1	Off	Off	On	On
	2	Off	Off	On	On
	1,2	Off	Off	On	On

Table 7. Possible combination of contact positions of the two FCRS-1P2T switches for configuration 2.

		Switch 1			
		Off	1	2	1,2
Switch 2	Off	Off	Off	Off	Off
	1	On	On	Off	On
	2	Off	Off	On	On
	1,2	On	On	On	On

Table 8. Possible combination of contact positions of the two FCRS-1P2T switches for configuration 3.

		Switch 1			
		Off	1	2	1,2
Switch 2	Off	Off	Off	Off	Off
	1	Off	On	Off	On
	2	Off	Off	On	On
	1,2	Off	On	On	On

Table 9. Possible combination of contact positions of the two FCRS-1P2T switches for configuration 4.

		Switch 1			
		Off	1	2	1,2
Switch 2	Off	Off	Off	On	On
	1	On	On	On	On
	2	Off	Off	On	On
	1,2	On	On	On	On

Table 10. Possible combination of contact positions of the two FCRS-1P2T switches for configuration 5.

		Switch 1			
		Off	1	2	1,2
Switch 2	Off	Off	Off	Off	Off
	1	Off	On	Off	On
	2	On	On	On	On
	1,2	On	On	On	On

Table 11. Possible combination of contact positions of the two FCRS-1P2T switches for configuration 6.

		Switch 1			
		Off	1	2	1,2
Switch 2	Off	Off	Off	Off	Off
	1	Off	On	On	On
	2	Off	On	On	On
	1,2	Off	On	On	On

3.4 Controlling an electrical load from three locations

Suppose that three switches are used to control a light bulb in a room as in Fig. **15**. Each switch is located next to a door, one on the entrance, the second on exit 1, and the third on exit 2. The light can be controlled by any switch and has one of the two states, either on or off. In the case of traditional switches, two 1P2T and one 2P2T-R switches are needed. In the case of the new switches, two FCRS-1P2T and one FCRS-1P3T are needed. Fig.16 and Table 12 present all possible contact positions for the three conventional switches. Fig. **17**, Table 13 and Table 14 present a simple configuration of the proposed FCRS in a circuit and all the possible combinations of the contact positions. It is important to mention that such kind of circuits can have many different configurations which allow a more controllability of the electrical loads. However, in this section, just one configuration is presented as an example.

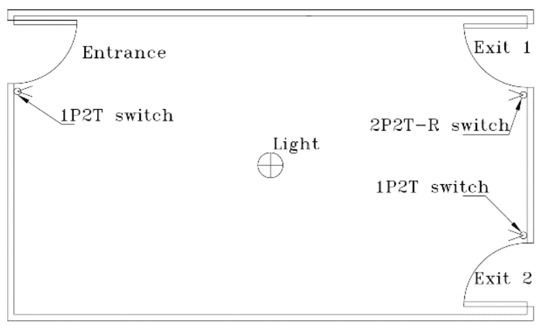

Fig. 15. Controlling a light in a room using two 1P2T and one 2P2T switches vs. two FCRS-1P2T and one FCRS-1P3T.

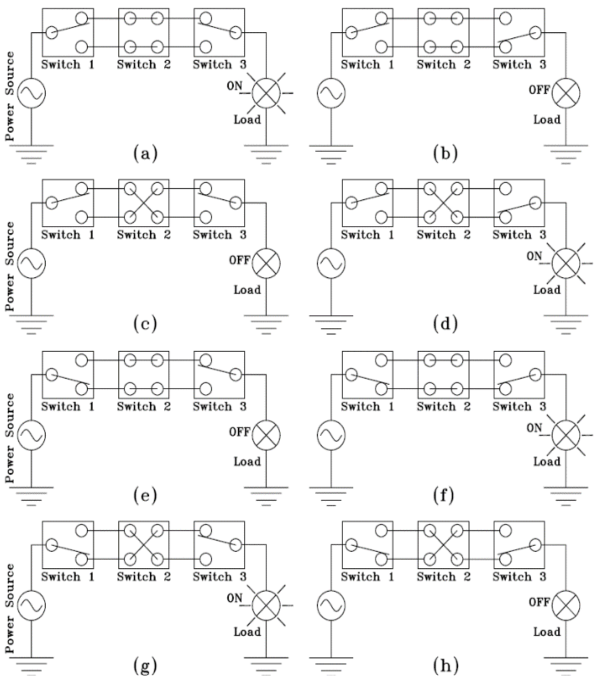

Fig.16. All possible contact positions for both switches of type 1P2T.

Table 12. Possible combination of contact positions of two 1P2T switches.

Switch 1	Switch 2	Switch 3	Light status
Position 1	Position 1	Position 1	On
Position 1	Position 1	Position 2	Off
Position 1	Position 2	Position 1	Off
Position 1	Position 2	Position 2	On
Position 2	Position 1	Position 1	Off
Position 2	Position 1	Position 2	On
Position 2	Position 2	Position 1	On
Position 2	Position 2	Position 2	Off

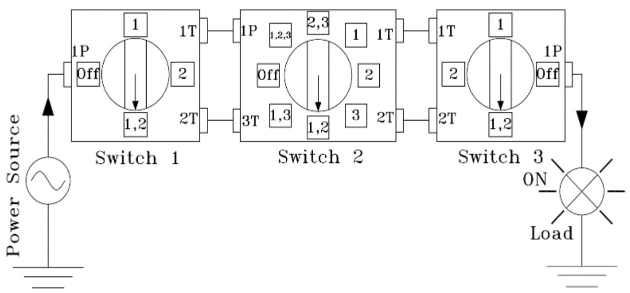

Fig. 17. A simple configuration of the circuit using FCRS.

Table 13. Possible combination of contact positions of two FCRS-1P2T and one FCRS-1P3T switches (Part 1).

Switch 1	Switch 2	Switch 3	Light status		Switch 1	Switch 2	Switch 3	Light status
0	0	0	Off		1	0	0	Off
0	0	1	Off		1	0	1	Off
0	0	2	Off		1	0	2	Off
0	0	1,2	Off		1	0	1,2	Off
0	1	0	Off		1	1	0	Off
0	1	1	Off		1	1	1	On
0	1	2	Off		1	1	2	Off
0	1	1,2	Off		1	1	1,2	On
0	2	0	Off		1	2	0	Off
0	2	1	Off		1	2	1	Off
0	2	2	Off		1	2	2	On
0	2	1,2	Off		1	2	1,2	On
0	3	0	Off		1	3	0	Off
0	3	1	Off		1	3	1	Off
0	3	2	Off		1	3	2	Off
0	3	1,2	Off		1	3	1,2	Off
0	1,2	0	Off		1	1,2	0	Off
0	1,2	1	Off		1	1,2	1	On
0	1,2	2	Off		1	1,2	2	On
0	1,2	1,2	Off		1	1,2	1,2	On
0	1,3	0	Off		1	1,3	0	Off
0	1,3	1	Off		1	1,3	1	On
0	1,3	2	Off		1	1,3	2	Off
0	1,3	1,2	Off		1	1,3	1,2	On
0	2,3	0	Off		1	2,3	0	Off
0	2,3	1	Off		1	2,3	1	Off
0	2,3	2	Off		1	2,3	2	On
0	2,3	1,2	Off		1	2,3	1,2	On
0	1,2,3	0	Off		1	1,2,3	0	Off
0	1,2,3	1	Off		1	1,2,3	1	On
0	1,2,3	2	Off		1	1,2,3	2	On
0	1,2,3	1,2	Off		1	1,2,3	1,2	On

Table 14. Possible combination of contact positions of two FCRS-1P2T and one FCRS-1P3T switches (Part 2).

Switch 1	Switch 2	Switch 3	Light status		Switch 1	Switch 2	Switch 3	Light status
2	0	0	Off		1,2	0	0	Off
2	0	1	Off		1,2	0	1	Off
2	0	2	Off		1,2	0	2	Off
2	0	1,2	Off		1,2	0	1,2	Off
2	1	0	Off		1,2	1	0	Off
2	1	1	Off		1,2	1	1	On
2	1	2	Off		1,2	1	2	Off
2	1	1,2	Off		1,2	1	1,2	On
2	2	0	Off		1,2	2	0	Off
2	2	1	Off		1,2	2	1	Off
2	2	2	Off		1,2	2	2	On
2	2	1,2	Off		1,2	2	1,2	On
2	3	0	Off		1,2	3	0	Off
2	3	1	Off		1,2	3	1	Off
2	3	2	Off		1,2	3	2	Off
2	3	1,2	Off		1,2	3	1,2	Off
2	1,2	0	Off		1,2	1,2	0	Off
2	1,2	1	Off		1,2	1,2	1	On
2	1,2	2	Off		1,2	1,2	2	On
2	1,2	1,2	Off		1,2	1,2	1,2	On
2	1,3	0	Off		1,2	1,3	0	Off
2	1,3	1	On		1,2	1,3	1	On
2	1,3	2	Off		1,2	1,3	2	Off
2	1,3	1,2	On		1,2	1,3	1,2	On
2	2,3	0	Off		1,2	2,3	0	Off
2	2,3	1	Off		1,2	2,3	1	Off
2	2,3	2	On		1,2	2,3	2	On
2	2,3	1,2	On		1,2	2,3	1,2	On
2	1,2,3	0	Off		1,2	1,2,3	0	Off
2	1,2,3	1	On		1,2	1,2,3	1	On
2	1,2,3	2	On		1,2	1,2,3	2	On
2	1,2,3	1,2	On		1,2	1,2,3	1,2	On

3.5 Comparison between the traditional switches and FCRS

In this subsection, a comparison between traditional switches and FCRS is presented in Table 15. FCRS can control many electrical loads simultaneously which is not the case of any other traditional switch. For example, in the case of 1P2T switch, maximum two loads an be controlled and only one of them can be turned on or off. However, FCRS-1P2T can turn off all loads, turn on load 1, turn on load 2, and turn on loads 1 and 2, which is not the case of any other switch. In addition, the FCRS can have a large number of configurations which allow one switch to overtake the control not only on the electrical loads, but also on other switches in the same circuit, which will increase the security, privacy, and satisfaction of a certain user, while reducing the conflict between multi-users who are trying to control the same load using many switches on the same circuit. However, FCRS present complicated configuration that might increase the complexity of the manufacturing and the system, which are considered its main drawbacks. Despite the mentioned limitations, FCRS can replace one or many switches and protection devices, which will reduce the investment cost. Hence, it is more attractive to a specific type of users.

Table 15. Comparison between traditional switch and FCRS.

Description	Traditional switch	FCRS
Control many electrical loads at a time	No	Yes
Control other switches on the same circuit	No	Yes
Increase the satisfaction of the user	Maybe	Yes
Increase the security while repairing the electrical load	No	Yes
Reduce the conflict between multi-users	No	Yes
Increase the privacy of the user	No	Yes
System is less complex	Yes	No
Manufacturing of the switch is less complex	Yes	No
Low manufacturing cost	Yes	No
Reduce the investment cost by reducing the number of installed switches and protection devices	No	Yes
Simple configuration and installation	Yes	No

4. CONCLUSION

Nowadays, electromechanical switches are widely deployed and used in buildings, in which they can turn on and off one or many electrical loads by changing the position of contacts. The most used switches are single-pole single-throw (SPST), single-pole double-throw (SPDT), and double-pole double-throw (DPDT). Despite the utility of these kinds of switches in controlling electrical loads such as lighting, they have many limitations. The most common limitations are low security, low controllability, and low privacy when many users are trying to control the same load. Hence, there is a need to create a novel switch which will give one or more of the users full control over a certain electrical load or circuit. To do so, this paper proposes a fully controllable rotary switch (FCRS) in which it gives single or many users partial or full control over circuits and other switches. Thus, all the mentioned issues are solved, and one user is able to block others from controlling the electrical load, which is not the case of any other conventional switch. The FCRS is a rotary switch that has one pole and many throws (in one or many decks or layers) connected in complicated configurations to give the user full control of the electrical load and to block other users from controlling it even if many switches are a part of the same circuit. The FCRS has many advantages over the traditional switches, such as (a) increasing the security and privacy of the user by fully controlling the circuit even if other switches exist in the same circuit; (b) the user can give limited or no access to other users; (c) reducing the installation cost by avoiding the installation of protection devices such as disconnecting switches, and reducing the installation of additional switches. For validation purposes, FCRS is compared to other existing switches. Results show that installing FCRS in buildings can increase the performance of the user since it can give him full access over the load and also give him a range of priorities that he can choose. In conclusion, FCRS shows many advantages over the traditional switches and needs further investigations in other fields.

REFERENCES

[1] Farlex, "Switch," in *The Free Dictionary*, ed: Farlex, 2008.

[2] M. L. Murphy, "The American Heritage® Dictionary of the English Language," *Dictionaries: Journal of the Dictionary Society of North America*, vol. 22, pp. 181-199, 2001.

[3] C. Zhai, D. Hanaor, G. Proust, and Y. Gan, "Stress-dependent electrical contact resistance at fractal rough surfaces," *Journal of Engineering Mechanics*, vol. 143, p. B4015001, 2017.

[4] P. G. Slade, *Electrical contacts: principles and applications*: CRC press, 2017.

[5] R. Holm, *Electric contacts: theory and application*: Springer Science & Business Media, 2013.

[6] (2021, March 18). *Chapter 4 Switch Types*. Available: https://www.allaboutcircuits.com/textbook/digital/chpt-4/switch-types/

[7] EATON, "Switching Devices," vol. 2, EATON, Ed., ed. Canada: EATON, 2018, pp. 1-139.

[8] Simon, "Simon 82 Detail Catalogue," SIMON, Ed., ed. Spain: SIMON, 2016, pp. 1-96.

[9] (2015, March 19). *Types Of Switches*. Available: https://www.electronicshub.org/switches/

[10] C. Technologies, "Switches and Controls," C. Technologies, Ed., ed. United States of America: Carling Technologies, 2020, pp. 1-236.

[11] Berker, "Switches and Building Control Systems," Berker, Ed., ed. Germany: Berker, 2020, pp. 1-76.

[12] B. Formisano. (2021, March 17,). *4 Types of Electrical Switches in the Home*. Available: https://www.thespruce.com/types-of-electrical-switches-in-the-home-1824672

[13] W. Electronics. (2019, March 16,). *Types of Switches – Special Applications by Touch Control*. Available: https://www.watelectronics.com/types-of-switches-with-applications/

[14] EleProCus. (2021, MArch 15). *Switches – Types & Working*. Available: https://www.elprocus.com/switches-types-working/

[15] Legrand, "Products and Systems for Electrical and Digital Building Infrastructures," LEGRAND, Ed., ed. France: Legrand, 2015, pp. 1-835.

[16] ABB, "Electrical installation solutions for buildings Product news 2020," ABB, Ed., ed. Germany: ABB, 2020, pp. 1-242.

[17] S. Electric, "Asfora Catalog 2020," S. Electric, Ed., ed. France: Schneider Electric, 2020, pp. 1-30.

[18] Y. Kouzaki, K. Yamasawa, and H. Nakamura, "A new centrifugal switch using magnetic fluid," *Journal of Magnetism and Magnetic Materials*, vol. 65, pp. 393-396, 1987.

[19] Union-Connector. (2021, October 1,). *Company Switch for Portable Power Distribution Boxes*. Available: https://www.unionconnector.com/company-switch/

[20] Y.-S. Song, J.-H. Baek, T.-K. Ko, and Y.-K. Kim, "A Study of the Dead Man's Switch considering bio-response," in *Proceedings of the KSR Conference*, 2011, pp. 165-171.

[21] B. Scaddan, *IEE Wiring Regulations: Explained and Illustrated*: Routledge, 2008.

[22] E. Ramsden, *Hall-effect sensors: theory and application*: Elsevier, 2011.

[23] H. Cai, G. Ding, Z. Yang, Z. Su, J. Zhou, and H. Wang, "Design, simulation and fabrication of a novel contact-enhanced MEMS inertial switch with a movable contact point," *Journal of Micromechanics and Microengineering,* vol. 18, p. 115033, 2008.

[24] M. Wei, Z. Yitshak, and W. Man, "Design and characterization of inertia-activated electrical micro-switches fabricated and packaged using low-temperature photoresist molded metal-electroplating technology," 2020.

[25] H. Olovsson and J. Constantinescu, "Application of Disconnecting Circuit-Breakers," *Report ID,* vol. 427.

[26] R. M. Marston, *Security Electronics Circuits Manual*: Newnes, 1998.

[27] J. L. Schum, *Electronic locking devices*: Butterworth-Heinemann, 1988.

[28] T. S. El-Bawab, *Optical switching*: Springer Science & Business Media, 2008.

[29] C. Gorse, D. Johnston, and M. Pritchard, *A dictionary of construction, surveying, and civil Engineering*: Oxford University Press, 2012.

[30] R. A. Lacerda, "Flexible Membrane Switch Keyboard Graphic Overlay for Equipment," *Revista da Escola de Enfermagem da USP,* vol. 43, pp. 237-244, 2009.

[31] C.-Y. Jin and O. Wada, "Photonic switching devices based on semiconductor nano-structures," *Journal of Physics D: Applied Physics,* vol. 47, p. 133001, 2014.

[32] S. F. Barrett and D. J. Pack, "Atmel avr microcontroller primer: Programming and interfacing," *Synthesis Lectures on Digital Circuits and Systems,* vol. 7, pp. 1-244, 2012.

[33] Available: By [[:en:User:{{{1}}}|{{{1}}}]] at the English-language Wikipedia, CC BY-SA 3.0, https://commons.wikimedia.org/w/index.php?curid=11166282

[34] B. Stein, J. Reynolds, and W. J. McGuinness, *Mechanical and electrical equipment for buildings*: J. Wiley & Sons, 1992.

[35] midwestelectric.com. *Transfer Switches*. Available: https://www.midwestelectric.com/products/transfer-switches/transfer-switches-0

Research Article *Energy, Environment and Storage* (2022) 02-01-11:14

Energy, Environment and Storage

Journal Homepage: www.enenstrg.com

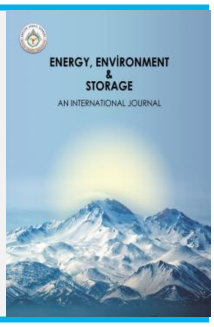

Testing of Pine Oil and Glycerol Ketal as Components of B10 Fuel Blend

Ibrahim Mamedov[1*], Sahila Huseynova[1], Ofelia Javadova[1], Nargiz Azimova[2], Rahila Huseynova[1], Shargiya Gasimova[1]

[1]*Baku State university, Faculty of chemistry, Z. Khalilov 23, Baku, Azerbaijan* [1*]*ORCID: 0000-0002-5757-9899*

[2]*Baku State university, Faculty of chemistry, Z. Khalilov 23, Baku, Azerbaijan* [2]*ORCID: 0000-0003-1276-5935*

ABSTRACT. The aim of the present work was to the preparation of biodiesel from sunflower oil and ethanol by the transesterification reaction in the presence of the KOH. The conversion was 88% at using a 1:3 molar ratio of oil to alcohol at 75°C. Important fuel physical properties of B10 blend with (or without) oxygenated additivities by the ASTM standards had been investigated. Based on the obtained results is noted that the fuel blend B10 with (or without) additivities has greater potentials for diesel engines than, B100 and fossil diesel.

***Keywords:** :* Transesterification, Biofuel, Biodiesel, Pine oil, Ionic liquid

Article History: Received:17.09.2021; Revised: 11.10.2021; Accepted:19.10.2021; Available online: 20.10.2021
Doi: https://doi.org/10.52924/SMQS5726

1. INTRODUCTION

Today there are serious environmental problems on Earth, such as the depletion of the ozone layer, the formation of acid rain, the accumulation of toxic chemicals in the upper atmosphere, the greenhouse effect and so on, which their formation have a significant role an automobile park of the world. Another problem is the exhaustion of petroleum, natural gas, etc. resources [1-4].

The development of new types of alternative biofuels sources is an actual problem of the modern world. Potential advantages of alternative biofuels for internal combustion engines are low emissions, longer engine life due to better lubrication, biological decomposition, high octane-cetane number, etc. In addition, biofuels do not emit toxic substances that cause environmental problems due to the absence of aromatic, nitrogen and sulfur compounds. One of the alternative types of fuel is biodiesel for diesel engines [5-8].

Alkaline catalytic systems are used in biodiesel industry, which leads to the formation of foam during cleaning, the formation of wastewater as a result of excessive washing. The choosing of the new catalytic systems is still relevant today in the production of biodiesel [9-12].

Besides indicated, the choosing of the new renewable raw materials sources also is a topical issue in the biodiesel industry [13].

2. MATERIALS AND METHODS

All the chemicals for the synthesis of glycerol ketal were obtained from commercial sources (Aldrich) and used as received.

Samples of diesel fuel, sunflower and pine oil were purchased at a fuel station and markets in Baku, Azerbaijan. The B10 blends with (or without) oxygenated additivities were prepared by mixing diesel and biodiesel (Figure 1, 2).

NMR experiments have been performed on a BRUKER FT NMR spectrometer (UltraShieldTM Magnet) AVANCE 300 (300.130 MHz for ^{1}H and 75.468 MHz for ^{13}C) with a BVT 3200 variable temperature unit in 5 mm sample tubes using Bruker Standard software (TopSpin 3.1). The ^{1}H and ^{13}C chemical shifts were referenced to internal tetramethylsilane (TMS); the experimental parameters for ^{1}H: digital resolution = 0.23 Hz, SWH = 7530 Hz, TD = 32 K, SI = 16 K, 90^0 pulse-length = 10 μs, PL1 = 3 dB, ns-= 1, ds= 0, d1 =1 s; for ^{13}C: digital resolution = 0.27 Hz, SWH = 17985 Hz, TD = 64 K, SI = 32 K, 90^0 pulse-length = 9 μs, PL1 = 1.5 dB, ns= 100, ds= 2, d1= 3 s. NMR-grade acetone-d_6 and $CDCl_3$ were used for the analysis of glycerol ketal and fuel blends.

The purity of the synthesized compounds was confirmed by thin-layer chromatography (TLC) on commercial aluminum-backed plates of silica gel (60 F254), iodine vapor was used as a visualizing agent, eluent- 5:2 hexane/ethyl acetate.

*Corresponding author: *bsu.nmrlab@gmail.com*

Fig. 1. Pine oil and glycerol ketal

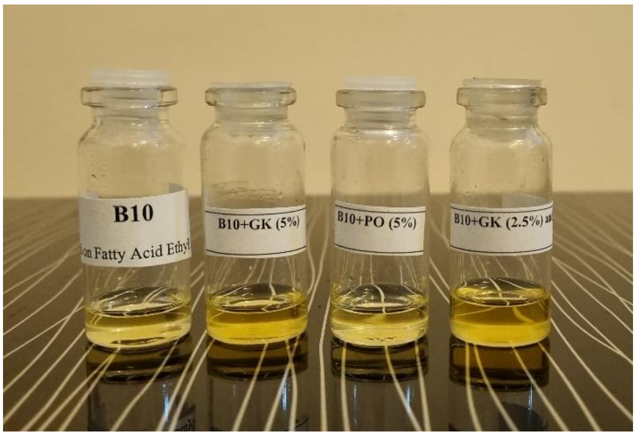

Fig. 2. The prepared fuel blends

2.1. The procedure for preparation of biodiesel

Sunflower biodiesel (B100) was obtained by dissolving 0.69 g KOH in 37.5 ml of ethanol (C_2H_5OH) without heating (at room temperature). After complete dissolution, 50 g of oil was added to this mixture. The reaction was carried out in a conical flask equipped with a reverse refrigerator and magnetic stirrer for 7 hours at 75 ºC (rotation speed was maintained at 1000 rpm). After stirring, the reaction mass was aged for at least 12 hours in dividing funnel. The reaction mass was divided into 2 layers using a dividing funnel: the upper layer contained biodiesel, the lower layer-glycerine. Untreated biodiesel was repeatedly washed with water in order to remove catalysts. The conversion rate was 88% when using the molar ratio of oil to ethanol 1:3 (Figure 3).

Fig. 3. The preparation of the biodiesel

Biodiesel synthesized from sunflower oil and its blends were characterized in accordance with the American Standard of Testing and Materials (ASTM) methods.

2.2. The procedure for preparation of glycerol ketal (GK)

A mixture of 25 g of pure glycerol, 100 ml of cyclopentanone, 0.75 g of p-toluenesulfonic acid (PTSA) was placed in a 500 ml conic flask fitted a reflux condenser and magnetic stirrer. The reaction mixture was stirred under 100°C for 5 working days. After the completion of the reaction mixture was neutralized with 0.5 g sodium acetate. In the next stage filtration and evaporation of the acetone had been carried out. The ketal was obtained by vacuum distillation, yield 96%.

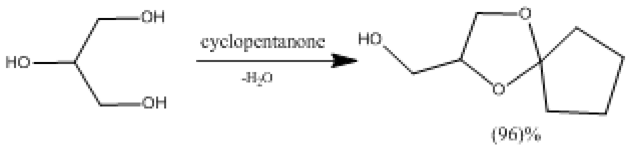

3. RESULT AND DISCUSSION

In our previous work [12] about the preparation of methanol biodiesel catalyzed by new ionic liquid system had been informed. Reporting work devoted to the preparation of ethanol biodiesel from the sunflower oil by the transesterification reaction in the presence of the KOH and testing of different fuel blends with the glycerol ketal and pine oil additivities.

The used feedstock sunflower physicochemical properties are shown in Table 1.

As known from the literature oxygenated compounds, such as glycerol ketals, pine oil (PO), etc. can be used as a fuel additive to reduce particulate emission and to improve the cold flow properties of liquid transportation fuels. It helps to reduce gum formation, improves oxidation stability, etc. [14, 15].

Table 1 Major fatty acids and physical properties of the refined sunflower oil

Fatty acid composition (wt.%)	16:0	18:0	18:1	18:2
	3.5–7.6	1.3–6.5	14–43	44–74
Acid value (mg of KOH/g)	0.28±0.5			
Saponification value (mg KOH/g)	193.3±0.5			
Iodine value (g I_2 per 100 g)	121.4±0.5			
Viscosity (cP)	34.1±0.5			
Flash point (°C)	265			
Pour point (°C)	+12			
Density (g/cm^3)	0.9186			

Considering the above indicated, the properties B10 blend (based on ethanol) in presence of cyclopentanone ketal and pine oil were studied. Pine oil can be regarded as one of the less viscous fuels in the likes of ethanol, methanol and consists of mainly cyclic terpene alcohols, known as terpineol ($C_{10}H_{18}O$) along with alpha-pinene ($C_{10}H_{16}$).
The physical properties of the diesel, sunflower biodiesel (B100), B10 blends with (or without) oxygenated additivities were investigated and the results are shown in Table 2, 3.

Table 2 The physical properties of B100, B10 and diesel fuels

Properties	**ASTM Methods**	**ASTM diesel**	**ASTM biodiesel**	**diesel**	**B10**	**B100**
Relative density at 20°C, g/cm^3	D1298	0.8-0.84	0.86-0.9	0.837	0.85	0.88
Viscosity at 40°C, mm^2/s, min-max.	D445	2-5	3.5-5.0	3.44	3.4	4.6
Flash point, °C, min.	D93	65	>120	70	110	180
Cloud point (°C)	D2500	-12	<20	7	5	15
Pour point (^{0}C)	D2500	-15	<15	0	-10	3
Iodine value g (l$_2$)/100 g	-	60-135	<120	1.58	46.6	112.5
Sulfur, ppm, max.	D 975-14	15	15	50	35	0
Water and sediment, vol%, max.	D 975-14	0.05	0.05	0	0	0
Copper corrosion, 3 hr at 50°C, max.	D 975-14	№3	№3	№2	№1	№1
Cetane number, min.	D 975-14	40	47	53	52.3	48.3

Table 3 The physical properties of the **B10** with the **GK** and **PO**

Properties	**B10**	**B10+PO (5%)**	**B10+GK (5%)**	**B10+GK (2.5%) and PO (2.5 %)**
Relative density at 20°C, g/cm^3	0.88	0.85	0.86	0.86
Viscosity at 40°C, mm^2/s, min-max.	4.6	3.7	3.4	3.5
Flash point, °C, min.	110	110	105	105
Pour point (^{0}C)	15	-4	-4	-4
Cloud point (°C)	3	-14	-18	-19
Iodine value g (l$_2$)/100 g	112.5	47.3	45.5	47.7
Sulfur, ppm, max.	35	34	34	34
Water and sediment, vol%, max.	0	0	0	0
Copper corrosion, 3 hr at 50°C, max.	№1	№1	№1	№1

As seen from the tables 2, 3 density decreased for the B10+PO, B10+GK and B10+GK+PO blends. According to the dependence between the density and kinematic viscosity also significantly decreases in the presence of 5% oxygenated compounds in the blends. The significantly decreasing of the viscosity to positive influences on the flow and sprays characteristics in the engine.

The flash points are decreased for the biodiesel blends than pure biodiesel (B100). The cloud and pour points of the B10 are increased, but the presence of GK and PO are significantly decreased for the B10+PO, B10+GK and B10+GK+PO blends.

The amount of sulfur significantly was decreased as the percentage of biodiesel, cyclic ketal and pine oil in blends from the 50 up to 34 ppm, which is very important for the environment and human health. As shown in our experimental results, water and sediment, also copper corrosion parameters are excellent.

The density, viscosity, flash-, pour-, cloud points, copper corrosion and etc. properties of investigated fuel blends are according to the diesel fuel standard and suggested blends can be used in diesel engines without any problems.

4. CONCLUSION

The properties of diesel, B100, B10 blends with (or without) glycerol ketal and pine oil were investigated on the ASTM standards.

Obtained results have demonstrated improvements of the important physical properties- such as density, viscosity, amount of sulfur, copper corrosion, flash-, pour- and cloud points for B10 fuel with (and without) oxygenated compounds.

An interesting aspect of the presented work is that this research was conducted for the first time on ethanol biodiesel.

Summarized the obtained data, we can note that the fuel blend B10 with (or without) oxygenated compounds have greater potentials for diesel engines than pure biodiesel (B100) and commercial diesel fuel.

REFERENCES

[1]]Barman, S.C., Kumar, R., Singh, G.S, et al. Assessment of urban air pollution and its health impact, *J. Enviro. Bio*., 31, 913-920, 2010.

[2] Janaun, J., Ellis, N. Perspectives on biodiesel as a sustainable fuel, *Renew.Sust. Energy Re*v.,14, 1312-1320, 2010.

[3] Meher, L.C., Vidya, D.S., Naik, S.N. Technical aspects of biodiesel production by transesterification-a review, *Renew. Sust. Energy Rev*., 10, 248-268, 2006.

[4] Miriam, D.T, Gonzalo, J., Jose, A.M., Elísabet, P., Mario, S. Glycerol ketals: Synthesis and profits in biodiesel blends, *Fuel*, 94, 614-6162, 2012.

[5] Edgar, L., Yiyan, L., Lopez, D.E., Suwannakaran, K., Bruce, D.A, James, G.J. Synthesis of biodiesel via acid catalysis, *Ind. Engineer. Chem. Res*., 44, 5353-5363, 2005.

[6] Nagarhalli, M.V., Nandedkar, V.M., Mohite, K.C. Emission and performance characterristics of Karanga biodiesel and its blends in a CI engine and its economics. *J. Engineer. Appl. Scien*., 5, 52-56, 2010.

[7] Nwafor, O.M.I. Emission characteristics of diesel engine operating on rapeseed methyl ester, *Renew. Enerergy*. 29, 119-129, 2004.

[8] Prasad, T.H., Reddy, K.H.C., Rao, M.M. Performance and exhaust emissions analysis of a diesel engine using methyl ester of oil with artificial neural network aid, *Inter. J. Engineer. Tech*., 2, 23-27, 2010.

[9] Kiakalaieh, A.T., Amin, N.A.S., Mazaheri, H. A review on novel processes of biodiesel production from waste cooking oil, *Appl. Energy*, 104, 683-710, 2013.

[10] Narasimharo, K., Lee, A., Wilson, K. Catalysts in production of biodiesel: A Review, *J. Bio. Mat. Bioenergy*, 1, 1-12, 2007.

[11] Lee, H.V., Juan, J.C., Taufiq-Yap, Y.H., Kong, P.C., Rahman, N.A. Advancement in heterogeneous base catalyzed technology: An efficient production of biodiesel fuels, *J. Renew. Sust. Energy*, 7, 1-47, 2015.

[12] Mamedov, I.G., Javadova, O.N., Azimova, N.V. Preparation of diesel fuel blends and study of their physical properties, *Proc. Univer. Appl. Chem. Biotech*., 2, 332-338, 2020.

[13] Singh, D., Sharma, D., Soni, S.L., Sharma, S., Sharma, P.K. A review on feedstocks, production processes, and yield for different generations of biodiesel, *Fuel*, 262, 1-15, 2020.

[14] Nanda, M.R., Zhang, Y., Yuan, Z., Qin, W., Ghaziaskar, H.S., Xu, C.C. Catalytic conversion of glycerol for sustainable production of solketal as a fuel additive: A review, *Renew.Sust. Energy Rev*.,56, 1022-1031, 2016.

[15] Prakash, T., Geo, V.E., Martin, L.J., Nagalingam, B. Evaluation of pine oil blending to improve the combustion of high viscous (castor oil) biofuel compared to castor oil biodiesel in a CI engine, *Heat Mass Tran*s., 55, 1491-1501, 2019.

Research Article

Energy, Environment and Storage (2021) 02-01:15-19

Energy, Environment and Storage

Journal Homepage: www.enenstrg.com

Country Border Line Control of Autonomous Rotary Wing Aircraft that Can Detect and Track Moving Objects

Tuğrul Oktay[1], Enes Özen[2*]

[1] *Erciyes Univ., Faculty of Aeronautics and Astronautics, Dept. of Aeronautical Eng.,Kayseri, Turkey, ORCID: 0000-0003-4860-2230*

[2*] *Hasan Kalyoncu University, Vocational School, UAV Technology and Operation, Gaziantep, Turkey, ORCID: 0000-0001-7816-2374*

ABSTRACT. Autonomous systems are widely used in missions that require continuity and high attention. The most important of these is the control of borders, which is a national security problem. It is done with PTZ (Pan Tilt Zoom) cameras located in the watch towers of the country's land borders, moving objects (human, vehicle, etc.) can be detected and this data is analyzed and converted into information in the relevant unit. In countries with very large land borders, installing such watchtowers would result in very high costs. Instead, this can be achieved with low-cost, low-altitude rotary wing aircraft. In this study, a system that can perform target detection and tracking is implemented thanks to the rotary wing aircraft that can perform this task and the imaging system it has on it.

Keywords: Rotary Wing Aircraft, Image processing, Target Detection and Tracking, Unmanned Aerial Vehicle System

Article History: Received:28.09.2021; Revised: 11.11.2021; Accepted:15.11.2021; Availableonline: 22.11.2021
Doi: https://doi.org/10.52924/ZURR2598

1. INTRODUCTION

By sensing the signals sent from the ground control station, the unmanned aerial vehicle enables it to guide and cruise in the air by changing the control surfaces in fixed-wing aircraft and rotor rotation speeds in rotary-wing aircraft. Another method is to load the previously specified task on the aircraft to the flight computer and navigate by generating signals to the relevant actuators by using the data it receives from the sensors it has on it [1]. Unmanned aerial vehicles are used for tasks such as search, rescue and surveillance in order not to put the human element at risk, in environments that require continuity, where terrorist elements are intense and chemical wastes are present, thanks to the useful loads they carry. An aircraft is an unmanned aerial vehicle system with its ground control station and its payload [2]. Unmanned aerial vehicles are used to increase agricultural productivity thanks to their cruising speed and ability to move independently from the ground. By placing the image processing feature on aircraft, real-time data analysis and transfer are realized, and studies are carried out to increase agricultural spraying and productivity [3]. High-altitude and long-range unmanned aerial vehicles used to provide border security are costly [4].

In this study, the unmanned aerial vehicle system developed for border security needs a more affordable budget, which makes the project advantageous. More than one aircraft in a given region can be commanded from a single ground control station. In this way, it is desired that more than one rotary wing, low-cost aircraft alternately scan and control the region, which will perform the task of the aircraft, which can cruise at high altitudes and observe the wider region. Thanks to the sensors it has on the aircraft, it will be able to instantly transmit battery information, flight time and location information to the ground unit, and will return to its base for the resupply process in order to be able to operate again. Thanks to the set containing more than one aircraft, it will be able to perform uninterrupted zone control.

* Corresponding author: enes.ozen@hku.edu.tr

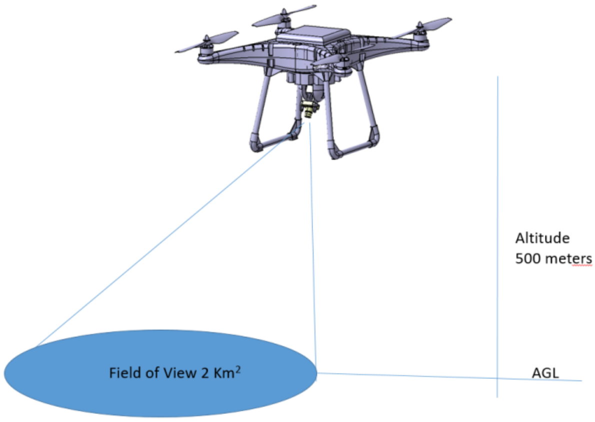

Fig. 1. Unmanned Aerial Vehicle Imaging System

2. MATERIALS AND METHODS

Unmanned aerial vehicles are classified according to their weight. Aircrafts weighing between 500-4000 gr are classified as UAV 0 category. Aircraft weighing between 4 and 25 kg are classified in the UAV 1 category. Aircrafts weighing between 25 and 150 kg are classified in the UAV 2 category. Aircraft with a weight of 150 kg or more are classified in the UAV 3 category [5]. In this study, the necessary programs for the control and analysis of movements with a quadrotor unmanned aerial vehicle, gimbal and ground control station were used. Quadrotor aircraft has advantages over other configurations in terms of ease of manufacture and maintenance.

Unmanned aerial vehicles can provide remote observation and intervention in cases where nuclear wastes are accessible so that people are not harmed in risky situations, to examine the situation of the fire during a fire and to perform the response more effectively. The increase in the world population increases the need for food. Efficiency needs to be increased in order to meet this need. For this, the costly spraying process should be done at a sufficient level, both the spraying costs can be reduced and the damage to the plants can be prevented. The most appropriate form of application can be achieved by adding the image processing capability to ensure that the drugs are applied to the most suitable parts, and it can be applied much faster than the manpower to apply. To achieve these, unmanned aerial vehicles are used. Rotary wing aircraft are suitable for this work. Thanks to its ability to hang in the air during spraying and imaging, a more effective task can be performed in the task area. In this study, the detection and tracking of moving objects from 500 meters altitude is carried out. Thanks to the electro-optical camera and thermal camera on the aircraft, target detection is performed at low altitude, day or night. The movement in the image is selected instantaneously and this data is transmitted to the aircraft's guidance unit. The data processed here is processed by the controller and transmitted to the actuators and rotors, and the aircraft can create and follow a flight path to follow these objects. The control system diagram that enables these processes to take place is shown in figure 2.

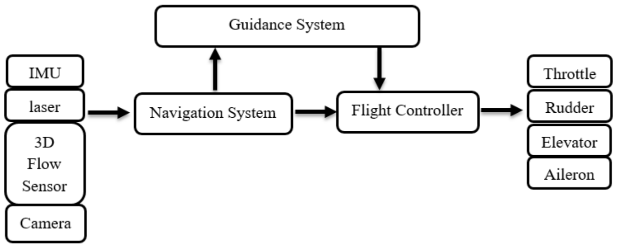

Fig. 2. Guidance, Navigation and Control Systems

The guidance system provides the orientation of the aircraft. It moves the airspace by creating the flight route and waypoints. While doing this, it also uses the data it receives from navigation and sensors [6]. In this way, flight safety is ensured and errors that may occur during navigation and tracking are reduced. It can move without the need for any direction command from the ground control station. At the same time, the imaging system modulates the image data to radio waves and transmits it to the antenna, thanks to the image transmission unit (Transmitter) on the aircraft. By means of the receiver unit on the ground, the operator on the ground can instantly follow this image from the ground and a warning can be sent to the relevant units.

2.1 Rotary Wing Aircraft Design

The principle of generating lift of rotary-wing aircraft, unlike fixed-wing aircraft, is achieved by positioning the rotors in a vertical position and rotating the propeller in a horizontal position. Multirotor aircraft, in order to zero the torque around the z-axis, as in helicopters, allows more than one rotor to rotate in different directions instead of the tail rotor, and the drag force and the torques created to balance each other and steer to their route. A controller is needed to control unstable rotary wing aircraft [7]. The reference signal enters the controller, the desired route is calculated and the rotational speeds of the rotors are determined. Since the rotation speeds of the rotors are controlled by the computer, the rotor configuration information must be introduced to the system and mounted accordingly. There are 2 types of configurations in quadrotor aircraft. These are given in Fig. 3 and 4.

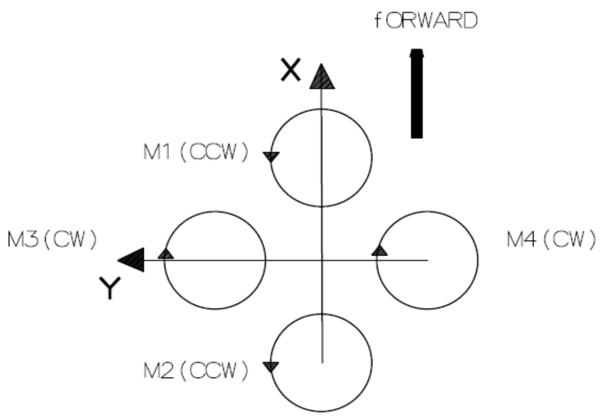

Fig.3. Quadcopter + Configuration

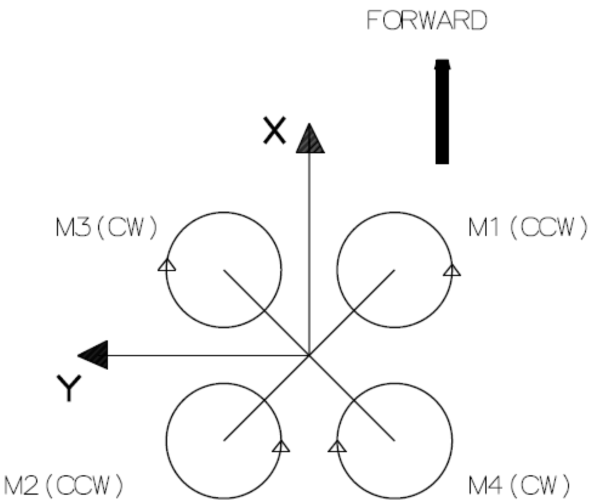

Fig. 4. Quadcopter X Configuration

Quadrotor aircraft consists of control board, ESC, engine and propellers. It is important that the propeller, motor and ESCs are chosen as equivalent, that the forces generated are the same, and that the responses to the signals are the same. In X configuration quadrotor aircraft, increasing the rotation speed of the rotors on the right causes the aircraft to lean to the left, that is, to perform a rolling motion. The faster rotation of the rear rotors according to the selected head position causes the air arc to move forward, that is, to make a pitching motion. It achieves this with a combination of rotation and linear motion around the axes according to the axis set placed in the center of gravity of the aircraft [8][12].

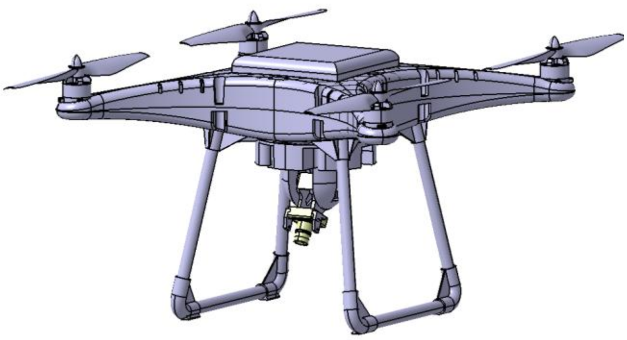

Fig.5. Isometric View of Quadcopter

Table 1 Quadcopter General Features

Wide	400 mm
Length	400 mm
Weight	3 kg
Flight Speed	75 km/h
Altitude	1500 feet
Flight Time	30 minutes
Payload	Sony 30X Electro-optic
Cost	20.000,00 TL

Unmanned aerial vehicles are equipped with payloads according to their purpose. In this study, target detection and tracking will be performed, so it is a payload camera system. Camera system; It consists of camera, image transmitter, antenna and 3 axis gimbal carrying them. gimbal; Independent of the aircraft, the camera performs pan-tilt-yaw movements around the axes of the axis set placed at the center of gravity. In this way, the aircraft can perform target tracking while suspended in the air within certain limits. In order to do this, a controller that can control the BLDCs on the axes is needed. Thanks to Alexmos and IMUs, which are very popular controllers in this regard, the aircraft can lock onto the target even while it is moving, and transmit this information to the flight controller.

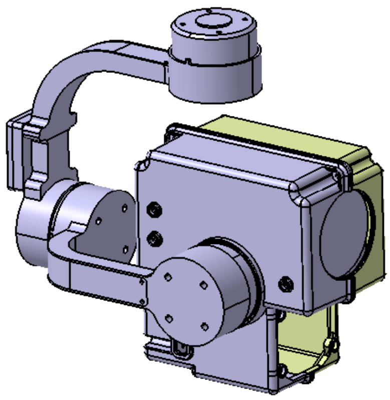

Fig. 6. 3 Axis Gimbal of Quadcopter

2.2 Image processing

Image processing is a set of operations that allow us to extract meaningful expressions from the image we have. These operations are performed by means of mathematical operations to be performed on the pixels that make up the image. After the image is obtained, an algorithm is designed according to the task to be done, and the image passes through these stages and fulfills the desired task. Any object can be detected and tracked on the image by using the necessary methods and algorithms according to the object to be detected. For example, in many countries abroad, the detection of criminals is carried out by this method. Any person can be detected through the images taken from the existing camera setups. Apart from this, it is also used in the traffic area. It can count the vehicles in the traffic and the speed of the vehicles can be measured. In this way, situations such as traffic density or excessive speed can be detected and necessary notifications can be made to the center. The quadcopter creates control commands to the aircraft with the help of the microcomputer and software, and the guidance system uses these commands to create a new route [10].

The stages of the signals that will be processed by the image obtained from the imaging system on the quadrotor and sent to the rotors by the controller are given in fig. 7.

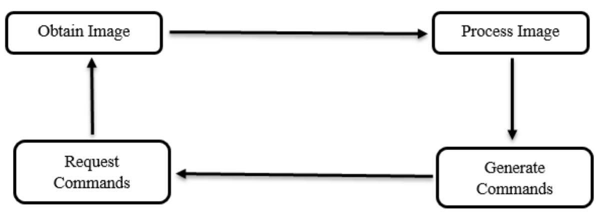

Fig.7. Image Processing Control System

The real-time images obtained are processed and compared with other sensors and previous data, as given in the flow in Figure 2, target detection and tracking is performed. Thanks to the data received from the navigation and sensors, the problems caused by image processing can be tolerated. In this way, the flight route to be created by the guidance system will prevent accidents.

Image processing method; It is defined as the application of digitally changing a picture taken with computer and software support. While image processing applications were initially used for military and security purposes, today they also serve sustainable and sensitive agriculture [10]. Three basic steps are important for the realization of image processing. The first of these is the conversion of the obtained image to digital format. The second step is to convert the obtained image to the desired format and edit it. The third and last step is to obtain results from the image by performing the necessary analysis. In order for an image to be processed digitally, first of all, data libraries must be created and transferred to the digital environment without any problems. After the existing data libraries have been created, it is time to process the selected images. Three different processing techniques are used for these.

The first of these is the histogram process, which is referred to as the white-gray balance. The aim here is to determine the shape in the image by using the white-gray balance in the digital image. In the second method, image filtering is used. In image filtering, it is aimed to use and process the desired part of the digital image by dividing it into grids. Thirdly, it is the definition of the digital image by using the RGB(red green blue) values based on the basic color model.

After choosing the right processing method, the selection of an ideal processing program (such as Matlab, phyton) and the processing of the data are carried out. The data obtained after processing needs to be interpreted and used. The data obtained with the technological developments are not only checked later, but can also be used with instant evaluations (real time) [11].

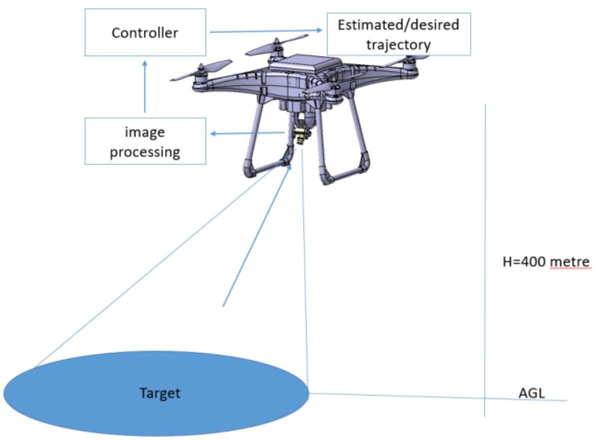

Fig.8. Vision-based tracking approach.

3. CONCLUSION

In this study, it is aimed to examine the studies on image recognition technology to design and implement the autonomous control system of the rotary wing aircraft and to prepare the academic ground for the aircraft developed for security to be used at the borders. The data obtained from the researches can be sent to the aircraft with the integrated camera system and image processing computer on the aircraft, and the ability to follow the target tracking can be gained thanks to the instant data received from other sensors and GPS. In this way, the long border line can be controlled without interruption by using more than one rotary wing aircraft.

In the next study, the necessary algorithm for the designed aircraft will be simulated in the MATLAB environment, and target detection, tracking and uninterrupted control of a certain region will be realized with the software obtained. Any object can be detected and tracked on the image by using the necessary methods and algorithms according to the object to be detected. For example, in many countries abroad, the detection of criminals is carried out by this method [13]. Any person can be detected through the images taken from the existing camera setups. Apart from this, it is also used in the traffic area. It can count the vehicles in the traffic and the speed of the vehicles can be measured. In this way, situations such as traffic density or excessive speed can be detected and necessary notifications can be made to the center.

REFERENCES

[1] K. Nonami, F. Kendoul, S. Suzuki, W. Wang, D. Nakazawa.(2010) *Autonomous Flying Robots*. Springer Tokyo Dordrecht Heidelberg London New York

[2] Austin, R.(2010). *Unmanned Aırcraft Systems Uavs Desıgn, Development And Deployment*. John Wiley & Sons Ltd, The Atrium, Southern Gate, Chichester, West Sussex, PO19 8SQ, United Kingdom

[3] Şin,B., Kadıoğlu,İ. (2019). *İnsansız Hava Aracı (İHA) ve Görüntü İşleme Teknikleri Kullanılarak Yabancı Ot Tespitinin Yapılması*. Turkish Journal of Weed Science 20(2):2019:211-217

[4] Valerdi, R. (2005). *Cost Metrics for Unmanned Aerial Vehicles*. September 2005, DOI: 10.2514/6.2005-7102

[5] SHGM. (2019). *İnsansız Hava Aracı Sistemleri Talimatı (Sht-İha)*

[6] Oktay,T, Özen, E. (2021). *Kapalı Ortamlarda Arama Kurtarma Görevi İçin Gelistirilen Şekil Değistirebilen Quadcopterin Sistem Modellemesi ve Tasarımı.* MAS 14th International European Conference On Mathematics, Engineering, Natural&Medical Sciences March 26-28, 2021/Széchenyi István University/HUNGARY

[7] Robert C. Leishman, John Macdonald, Randal W. Beard, Timothy W. McLain.(2014) *Quadrotors & Accelerometers State Estimation with an Improved Dynamic Model*. IEEE Control Systems Magazine. February

[8] O. Kose and T. Oktay, (2019) "Dynamic Modeling and Simulation of Quadrotor for Different Flight Conditions," *European Journal of Science and Technology,* no. 15, pp. 132-142.

[9] Ağın O., Malaslı Z. (2016). Görüntü işleme tekniklerinin sürdürülebilir tarımdaki yeri ve önemi: iteratür çalışması. Tarım Makinaları Bilimi Dergisi. 2016, 12 (3), 199-206.

[10] He L., Yanqiu N., Zhengzheng L. and Xiang F. (2016). *Quadcopter autonomous control system based on image recognition.* 2016 12th World Congress on Intelligent Control and Automation (WCICA) June 12-15, 2016, Guilin, China

[11] Şin B., Kadıoğlu İ., Sarı T. (2019). Detectıon and ıdentıfıcatıon of weed by ımage processıng techniques. BIALIC, 7-8 Novamber 2019, s. 40, Lviv Ukraine.

[12] Köse,O., Oktay,T.(2021) *İnovatif Yöntemlerle Kuadkopter Modellenmesi, Kontrolü Ve Gerçek Zamanlı Uygulamaları*. Doktora Tezi, Erciyes Üniversitesi, Fen Bilimleri Enstitüsü, KAYSERİ, 2021

[13] Laghari A., Asif R. (2017). Image Processing Based Proposed Drone for Detecting and Controlling Street Crimes. 2017 17th IEEE International Conference on Communication Technology

Research Article

Energy, Environment and Storage (2021) 02-01:20-33

Energy, Environment and Storage

Journal Homepage: www.enenstrg.com

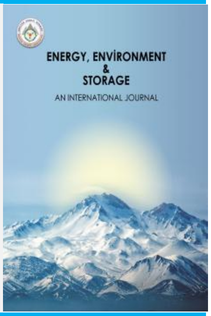

Novel Optimal Perennial Calendar Systems vs Gregorian Calendar and Their Impact on the Energy Demand and the Environment

Claude Ziad El-Bayeh [1*], Mohamed Zellagui[2], Brahim Brahmi[3]

[1] *Canada Excellence Research Chair Team, Concordia University, Canada, ORCID:* 0000-0002-8268-8878

[2] *Department of Electrical Engineering, Faculty of Technology, University of Batna, Fesdis, 05078, Batna, Algeria, ORCID:* 0000-0003-2558-2273

[3] *Electrical and Computer Engineering Department, Miami University, Oxford, USA, ORCID:* 0000-0002-4486-0710

ABSTRACT. Have you ever missed an event because you were confused about days and dates? Do you remember the date of any specific day without looking at the calendar? Is the current Gregorian Calendar efficient enough for usage, and does it facilitate our life or make it more complicated? Have you ever thought about a simpler way to calculate days and dates in a year without using a calendar? All these questions are answered in this paper, in which authors propose two contributions, (a) a new mathematical formula that calculates the number of days in any month in the Gregorian calendar for any year, including the leap years, (b) an original optimization method that creates optimal perennial calendars. Results show that there is more than one way to create a perennial calendar using the proposed optimization model, in which the number of days in each month does not change, neither the dates. Hence, all months have the same sequence of days and dates. In other meaning, Monday becomes the first day of every month, and Sunday becomes the last day. Consequently, the calendars become much easier to memorize, and it becomes simpler to predict the days and dates in any year. In addition, the proposed optimal perennial calendar system reduces the energy demand and pollution worldwide, in which it has less impact on the environment and climate change compared to the Gregorian calendar. This is due to the fact that less printed-out calendars are produced, and less time is spent on the digital calendars to check the dates and days.

Keywords: Gregorian Calendar; Weekly-based Calendar; Original Calendar; Optimization algorithm; Energy saving.

Article History: Received:04.10.2021; Revised: 08.11.2021; Accepted:15.11.2021 Available online: 22.11.2021.
Doi: https://doi.org/10.52924/WMPX7768

NOMENCLATURE

GC	Gregorian Calendar
IFC	International Fixed Calendar
JC	Julian Calendar
OPC	Optimal Perennial Calendar (Proposed in this paper)
PC	Perennial Calendar

1. INTRODUCTION

1.1 Background and motivation

From the early beginning of human civilizations, people realized the importance of organizing their daily life [1]. Many cultures created their calendars and dating systems that helped them to save religious and social activities and events [1]. The most recognized calendars in the ancient time include but are not limited to, Roman calendar [2], [3], Sumerian calendars [4], [5], Babylonian calendar [6], Zoroastrian calendar [7], Hebrew calendar [8], Hellenic calendars [9] and Julian calendar [10]. In the late sixteenth century, the Gregorian calendar (GC) was introduced by Pope Gregory XIII on October 15, and was later adopted worldwide [11]. In the Gregorian calendar, a year is composed of 12 months. Each month has a different number of days. For example, January has 31 days, February has 28 days, and 29 in a leap year, April has 30 days, and so on. One of the main critics of the Gregorian calendar is that it is very difficult to find a simple relationship between dates and days [12]. Sometimes, the dates become confusing especially when a particular day like Monday, is the first day in a month, and the second or even the seventh in another month; sometimes holidays which are on a specific date, such as December 24, could be located during the weekdays (e.g., Tuesday 24, 2019), while it can be in weekends in another year (e.g., Saturday 24, 2022). Hence, calculating days and dates is a difficult task, because of the irregularities in the Gregorian calendar. It appears that the existing calendar system becomes a little bit confusing for most of the people, and a much simpler calendar is needed. In addition, billions of calendars are printed every year worldwide, in which millions of trees are used every year to supply the demand. The emission of CO_2, the pollution, the

[*] Corresponding author: c.bayeh@hotmail.com

waste, and the energy used to print out Gregorian calendar cannot be neglected especially when around billions of calendars are thrown every year. Therefore, Gregorian calendar imposes negative impact on the society, the economy, and the environment, in which a solution should be proposed to facilitate the life of people and create a more sustainable and greener society.

Some questions may arise. What happens if we create a more organized calendar in which the days and dates in a month do not change? For example, Monday will always be the first day of any month. The holidays will have the same dates and days in any year, including leap years. For example, December 24, will always be on Wednesday, whatever is the year. Can we create an eco-friendly calendar, which is very easy to memorize without printing a hard copy to reduce pollution? Moreover, human beings always tend to develop and invent new things every day in order to facilitate their lives. So why do we not develop an easier way to count days, weeks, and months in a year?

1.2 Gregorian vs. Julian Calendars

A year is the time a given celestial object (e.g., Earth, Mars, etc.) takes to complete one orbit around another celestial object (e.g., Sun), also called the orbital period. However, astronomical years do not have integer numbers of days; for example, the Earth orbits the Sun in about 365.2425 days; therefore, it is necessary to introduce the intercalation system such as leap years. Julian and Gregorian calendars are the most common ones these days. A Julian calendar counts 365.25 days in a year, while 365.2425 days are considered in the Gregorian calendar. In total, a leap year occurs every four years in the Julian calendar, in which one day is added to the month of February. The Gregorian calendar follows almost the same concept; however, some new rules were added to reduce the gap with the reference (365.2422 days per year). These new rules are cited as follows:

> *"Every year that is exactly divisible by four is a leap year, except for years that are exactly divisible by 100, but these centurial years are leap years if they are exactly divisible by 400. For example, the years 1700, 1800, and 1900 are not leap years, but the years 1600 and 2000 are [13]."*

These new rules reduce the error by 1.2 days every 4,000 years, as shown in Table 1, while the Julian calendar shows an error of 31.2 days. From this place, the Gregorian calendar was adopted until this time.

Table 1. Accuracy comparison between Julian calendar and Gregorian calendar over a period of 4000 years.

Calendar	**Number of days in a year**	**Number of days in 4 years**	**Number of days in 400 years**	**Number of days in 4,000 years**	**Error per 400 years with respect to the reference**	**Error per 4,000 years with respect to the reference**
Julian	365.25	1,461	146,100	1,461,000	3.12	31.2
Gregorian	365.2425	1,460.97	146,097	1,460,970	0.12	1.2
Reference	**365.2422**	**1460.9688**	**146096.88**	**1,460,968.8**	**-**	**-**

1.3 International Fixed Calendar

The Gregorian calendar has serious problems and flaws. The main problem of the Gregorian calendar is that the number of days in months is not fixed, and it may vary between 28 and 31 days per month. Moreover, a month can start on Monday (June 1, 2020) and the next one on Wednesday (July 1, 2020). Therefore, there is no consistency between days and dates. The date of February 29 occurs every four years, which seems unpleasant to some people. Moreover, a year is divided into four quarters (3 months each quarter). If the number of days is counted in each quarter, it appears that the first quarter has 90 days, the second one has 91 days, and the third and fourth one has 92 days. The quarters are not symmetrically distributed. Therefore, two additional working days in a quarter can make a difference in the statistics for a big company. In addition, holidays are not stable during the year. For example, Christmas on December 24 is on Thursday in 2020, while it is on Saturday in 2022.

In conclusion, the Gregorian calendar is difficult to handle and memorize. To solve the problem, other sophisticated calendars were proposed to facilitate our lives. The most famous calendar is called International Fixed Calendar (IFC) and also called Cotsworth calendar, which was introduced by Moses Cotsworth in 1902 [14]. The calendar divides the solar year into 13 months of 28 days each. This kind of calendar is defined as a perennial calendar, in which every weekday has a fixed date every year. The IFC has some rules to follow, as described below [14]:

- One year has 13 months,
- Each month has exactly 4 weeks,
- Each week has 7 days. Therefore, the total number of days in a year becomes equal to 364 (7 days x 4 weeks x 13 months),
- An extra day is added as a holiday at the end of the year, and it is called Year Day,
- The Year Day does not belong to any week. Therefore, the total number of days, including the Year day in a year, becomes equal to 365 days,
- The Cotsworth calendar is correlated to the Gregorian calendar in which it has the same number of days, and each year starts on the same date, which is January 1,
- Cotsworth calendar has the same month's names and order as the Gregorian calendar, except the extra month (called Sol), which is inserted between June and July [15],
- A leap year has 366 days, and its occurrence follows the Gregorian rules,
- The Leap-Day is inserted on June 29 (between Saturday, June 28, and Sunday, Sol 1),
- Each month starts on a Sunday and ends on a Saturday,
- Both Year-Day and Leap-Day do not belong to any week. They are preceded and followed by a Saturday and a Sunday, respectively.

Table 2 presents the IFC, in which the Leap-Day and the Year-Day are added to the end of months June and December. Despite the success of this calendar, it received many critics, and it has some drawbacks. The most common critics can be presented as follows:

a. The calendar claimed to have exactly 28 days in each month. However, when the leap day is added, June month will contain 29 days and not 28. The same for the leap year, in which it is added to the month of December. Hence, the total number of days becomes equal to 29.
b. The calendar has 13 months, which is a prime number and cannot be divided by 2, nor by 3, neither by 4. Therefore, it becomes difficult to categorize activities based on a biannually, triannually, or quarterly basis. Thus, activities will be out of alignment with months.
c. The week starts with a Sunday. Hence, the calendar disagrees with ISO 8601, in which the first day is Monday and not Sunday.
d. Adding a day between Saturday and Sunday is considered confusing, especially when leap-day and year-day are added to the month of June and December.
e. Some people are pessimistic about the date Friday 13th.
f. The weekday starts on the second of each month and not on the first.

Table 2. International Fixed Calendar.

International Fixed Calendar

Proposed by Moses Cotsworth in 1908

January

S	M	T	W	T	F	S
1	2	3	4	5	6	7
8	9	10	11	12	13	14
15	16	17	18	19	20	21
22	23	24	25	26	27	28

February

S	M	T	W	T	F	S
1	2	3	4	5	6	7
8	9	10	11	12	13	14
15	16	17	18	19	20	21
22	23	24	25	26	27	28

March

S	M	T	W	T	F	S
1	2	3	4	5	6	7
8	9	10	11	12	13	14
15	16	17	18	19	20	21
22	23	24	25	26	27	28

April

S	M	T	W	T	F	S
1	2	3	4	5	6	7
8	9	10	11	12	13	14
15	16	17	18	19	20	21
22	23	24	25	26	27	28

May

S	M	T	W	T	F	S
1	2	3	4	5	6	7
8	9	10	11	12	13	14
15	16	17	18	19	20	21
22	23	24	25	26	27	28

June

S	M	T	W	T	F	S	Leap-Day
1	2	3	4	5	6	7	
8	9	10	11	12	13	14	
15	16	17	18	19	20	21	
22	23	24	25	26	27	28	29

Sol

Sun	Mon	Tue	Wed	Thu	Fri	Sat
1	2	3	4	5	6	7
8	9	10	11	12	13	14
15	16	17	18	19	20	21
22	23	24	25	26	27	28

July

S	M	T	W	T	F	S
1	2	3	4	5	6	7
8	9	10	11	12	13	14
15	16	17	18	19	20	21
22	23	24	25	26	27	28

August

S	M	T	W	T	F	S
1	2	3	4	5	6	7
8	9	10	11	12	13	14
15	16	17	18	19	20	21
22	23	24	25	26	27	28

September

S	M	T	W	T	F	S
1	2	3	4	5	6	7
8	9	10	11	12	13	14
15	16	17	18	19	20	21
22	23	24	25	26	27	28

October

S	M	T	W	T	F	S
1	2	3	4	5	6	7
8	9	10	11	12	13	14
15	16	17	18	19	20	21
22	23	24	25	26	27	28

November

S	M	T	W	T	F	S
1	2	3	4	5	6	7
8	9	10	11	12	13	14
15	16	17	18	19	20	21
22	23	24	25	26	27	28

December

S	M	T	W	T	F	S	Year-Day
1	2	3	4	5	6	7	
8	9	10	11	12	13	14	
15	16	17	18	19	20	21	
22	23	24	25	26	27	28	29

1.4 Does the Gregorian calendar have an impact on the environment and energy demand?

There has been a high awareness of global warming and climate change in recent years, where the average global atmosphere temperature has exceeded 1.2^{o}C above the pre-industrial level. Many countries and regions have started to shift from fossil fuel-based power plants to renewable energy-based power plants in order to reduce the Carbon footprint and the emission of CO_2 and other harmful gases [16, 17].

Fossil fuel-based power production is not the only cause of global warming and climate change. Inadequate consumption, excess of unnecessary production, and bad waste management also play an important role in increasing pollution and negatively affecting the whole planet [17, 18]. In addition, the competition between countries to increase their economic growth has also a huge impact on the Carbon footprint and the emission of harmful gases, which threaten the whole life on Earth [19]. From this place, any kind of production, whether it is energy or material, has a direct impact on the environment and climate change. More specifically, the excessive production of Gregorian calendars every year is energy-consuming and polluting at the same time since the whole process of production and distribution of the products consumes lots of energy and primary materials. According to The New York Times [20], the average number of printed calendars in households was 3.12 in 2011 compared to 3.98 in 1981 in the United States. Most of the countries still rely heavily on paper-based calendars.

With the advancement of technologies, digital calendars are presented everywhere, such as on smartphones, smart televisions, smartwatches, computers, laptops, etc. Even with the usage of these digital calendars, the time spent on surfing the calendars and looking for days and dates is considerably high. If the time used on such devices to check the calendar is summed up during a year for the whole world, the energy wasted is high enough to power a complete village for a complete year.

According to [21], and according to the standards ISO 14040/14044, the average carbon footprint of an office paper during its lifecycle is around 4.64gCO_2eq per A4 sheet. In this case, the weight of the sheet will be around 80g/m2. Therefore, a paper-based calendar which approximately has (200 A4 sheets or 400 A5 sheets) can produce about 928 gCO_2eq (or 0.928 kgCO_2eq).

Based on a survey released by a leading calendar communications platform in Australia in 2018, ECAL [22], 47% of participants rely on mobile calendars, 23.4% rely on a desktop calendar, 27.8% rely on paper calendars (including diary, journal, and planner), while 1.8% used other scheduling tools, as presented in Figure 1.

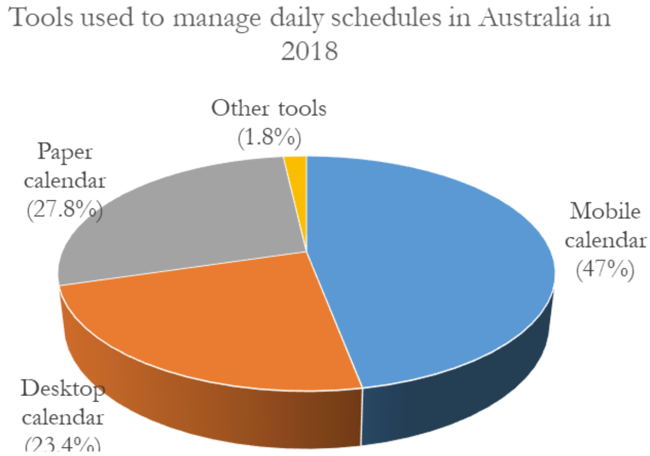

Figure 1. Tools used to manage daily schedules in Australia, 2018.

If these percentages are generalized on the total population on Earth (7.9 billion in 2021), just for approximation. It can be found that the number of produced paper-based calendars in a single year reaches about 2.2 billion paper-based calendars per year. Since the Carbon footprint of one paper-based calendar is about 0.928 kgCO_2eq, producing only paper-based calendars per year will be about 2.04 Mt CO_2eq (Mega tonne), which is a considerable amount. A more detailed calculation will be provided in this paper in the result section.

1.5 Contributions

The main contributions in this paper are stated as follows:

- A new mathematical formula is developed to describe the number of days in any month for any year (including leap year) for the Gregorian calendar. This formula eliminates the mistakes in counting the number of days in any month,
- Original perennial calendar systems are proposed, in which they respond to the critics mentioned in section 1.3 for the IFC. The proposed perennial calendar systems have the same number of days in any months, and the dates of days never change. For example, Monday will be always the first day of a week, a month and a year, and it will always have the same date (such as 1st January, 1st February, 1st March, etc.),
- A perfect calendar is newly introduced and defined as a calendar that can be divided into equal intervals during a year (e.g., 2 “biannual”, 3 “triannual”, 4 “quarter”, 5 “quinnanual”, and 6 “sexannual”), and each interval has exactly the same number of weeks and days.
- An original optimization algorithm that generates perennial calendars is proposed. An objective function and some constraints are defined for this purpose. The algorithm is solved with Mixed Integer Genetic Algorithm.

To validate our concept, one of the proposed perennial calendar systems is compared to the Gregorian calendar and the International Fixed Calendar, and different aspects are considered in the comparison, such as technical, economic, environmental, individual, and social aspects. Moreover, a deeper analysis is conducted to study their impact on energy consumption, energy and production waste, and the carbon footprint.

2. NEW MATHEMATICAL FORMULA DESCRIBES THE NUMBER OF DAYS IN ANY MONTH

Gregorian calendar is an irregular calendar in which the number of days is not the same for all months. Some months have 30 days, and others have 31. The month of February has 28 days, and a day is added in a leap year in which the total number of days becomes equal to 29. Sometimes, it is confusing for some people to remember the number of days for each month, and even it becomes embarrassing for others on social media to post wrong dates and days, such as in Figure 2.

Figure 2. Wrong date and day on a weather forecast show.

There is a traditional way to calculate the number of days in a month using the fist as in Figure 3. The knuckles of the four fingers of one's hand and the spaces between them can be used to remember the lengths of the months. By making a fist, each month will be listed as one proceeds across the hand. All months landing on a knuckle are 31 days long, and those landing between them are 30 days long, with variable February being the remembered exception. When the knuckle of the index finger is reached (July), go over to the first knuckle on the other fist, held next to the first (or go back to the first knuckle), and continue with August. This physical mnemonic has been taught to primary school students for many decades, if not centuries [23].

Figure 3. Traditional method uses the fist to count the number of days in a month.

Another method using the keyboard/piano is also popular, as presented in Figure 4. The cyclical pattern of month lengths matches the musical keyboard/piano alternation of wide white keys (31 days) and narrow black keys (30 days). The note F corresponds to January, and the diabolis in musica note F♯ corresponds to February, the exceptional 28-29 day month.

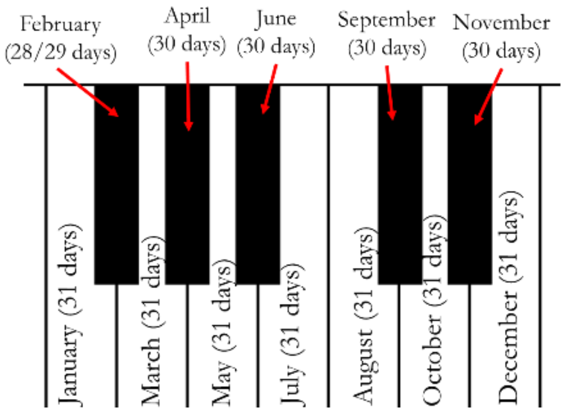

Figure 4. Traditional method uses the keyboard/piano to count the number of days in a month.

The disadvantages of the traditional methods are, (i) they are not based on mathematical proof, (ii) the number of days of February is not determined since they don't take into account the leap year. Although with these disadvantages, they are the simplest methods for counting the number of days in a month and have been taught for hundreds of years.

In the literature, there are various methods to calculate the day of the week for any particular date in the past or future [24, 25]. These methods rely on algorithms to determine the day of the week for any given date, including those based solely on tables as found in perpetual calendars that require no calculations to be performed by the user. A typical application is to calculate the day of the week on which someone was born or any other specific event occurred. Even by using the Gauss calendar formula, there are some parameters that should be predefined in order to calculate the number of days in a month.

In this paper, a new mathematical formula is proposed that calculates the number of days for each month even during a leap year, as presented in Eq. (1).

$$N_{days} = \begin{pmatrix} 30 + \dfrac{\cos(\pi(m-1+U(m-8)))+1}{2} \\ +rect_{0.2}(m-2)\left[rect_{0.2}\left(Mod(y,4)\right)-2\right] \end{pmatrix} \quad (1)$$

Where,

- N is the number of days in a month, i.e., 31 in January, 28 in February (in a non-leap year and 29 in a leap year), etc.,
- m is the month number, e.g., $m = 2$ for February,
- $U(x)$ is a unity step function defined in Eq. (2),
- $rect_T(x)$ is a rectangular function defined in Eq. (3),
- y is the year, e.g., $y = 2021$,
- Mod($number$, $divisor$) returns the remainder after a number is divided by a divisor. The result has the same sign as the divisor. Number: is the number for which you want to find the remainder, e.g, 2021. Divisor: is the number by which you want to divide the number, e.g, 4. For example, $Mod(1,4) = 1$, $Mod(2,4) = 2$, $Mod(4,4) = 0$, etc.

$$U(m-8) = \begin{cases} 1 \; if \; m \geq 8 \\ 0 \; if \; m < 8 \end{cases} \quad (2)$$

$$rect_T(x) = \begin{cases} 1 \; for \; -\dfrac{T}{2} < x < \dfrac{T}{2} \\ \dfrac{1}{2} for \; x = \pm\dfrac{T}{2} \\ 0 \; for \; -\dfrac{T}{2} > x > \dfrac{T}{2} \end{cases} \quad (3)$$

A step-by-step calculation is made in Table 3 to determine the number of days in any month of a year, including the leap year.

Table 3. Step by step calculation to determine the number of days in any month.

	January	**February**	**March**	**April**	**May**	**June**	**July**	**August**	**September**	**October**	**November**	**December**
Month (m)	**1**	**2**	**3**	**4**	**5**	**6**	**7**	**8**	**9**	**10**	**11**	**12**
Number of days	31	28 29	31	30	31	30	31	31	30	31	30	31
$U(m-8)$	0	0	0	0	0	0	0	1	1	1	1	1
$\cos(\pi(m-1+U(m-8)))$	1	-1	1	-1	1	-1	1	1	-1	1	-1	1
$\frac{\cos(\pi(m-1+U(m-8)))+1}{2}$	1	0	1	0	1	0	1	1	0	1	0	1
$30+\frac{\cos(\pi(m-1+U(m-8)))+1}{2}$	31	30	31	30	31	30	31	31	30	31	30	31
$rect_{0.2}(m-2)$	0	1	0	0	0	0	0	0	0	0	0	0
$rect_{0.2}(m-2)[rect_{0.2}(Mod(y,4))-2]$	0	-2 -1	0	0	0	0	0	0	0	0	0	0
$\left(\begin{matrix}30+\frac{\cos(\pi(m-1+U(m-8)))+1}{2}+\\ rect_{0.2}(m-2)[rect_{0.2}(Mod(y,4))-2]\end{matrix}\right)$	31	28 29	31	30	31	30	31	31	30	31	30	31

Remark: the number of days for the month of February in the table is 28 for non-leap year, and 29 for leap year.

Eq. (1) can be also programmed which makes it easier for the user to determine the number of days in each month for any year. The code is written in Scilab 6.1.1.

3. PROPOSED PERENNIAL CALENDAR

The idea of creating a perennial calendar, such as the International Fixed Calendar (IFC), was to make our life easier. Its main advantages are as follows: (a) the calendar never expires, and it is always relevant, (b) it becomes easier to memorize and remember events and dates, (c) there is no need to change the calendar or by a new one every year, (d) adding new events is easy and can be done once, etc. However, the IFC has many drawbacks, as mentioned previously. To address these drawbacks, new perennial calendar systems are proposed based on the idea of the IFC, the Gregorian calendar, and using optimization. To do so, a new annotation will be used in this paper to refer to a specific calendar. The annotation is "MWD+R", or simply the mathematical formula can be written as in Eq. (4), and explained in Figure 5.

Code on Scilab:

```
//Calculate the number of days in each month for any year

clear;clc;close;//Clear all previous data

repeat=1;//Initial value to enter the while loop

while repeat==1
    disp("Enter the year that you would like to check the
          number of days for each month");

    year=input("Year= ");

    for m=1:12 //m is the month number

        //convert a sign into a unit step function
        U=(sign(m-7.9)+1)/2;

        //convert a sign into a rectagular pulse function
        rect=(sign(m-2+0.2)+1)/2-(sign(m-2-0.2)+1)/2;

        rect_mod=(sign(modulo(year,4)+0.2)+1)/2-
                 (sign(modulo(year,4)-0.2)+1)/2;

        //Number of days for each month "m"
        N_days(m)=30+(cos(%pi*(m-1+U))+1)/2 + rect*
                      (rect_mod-2);
    end

    //Write the month number and the number of days in
     each month in the same matrix
    Number_of_Days_per_Month(1,:)=1:12;
    Number_of_Days_per_Month(2,:)=N_days';

    disp("Month Number:             ");
    disp("Number of days per month: ");
    disp(Number_of_Days_per_Month);

    disp("Would you like to repeat?");
    repeat=input("Press ""1"" for YES or any key for NO:
             ");
end

disp("Thanks for using this application!  ");
disp("************************************");
disp("Copyrighted (C) Claude Ziad El-Bayeh");
disp("************************************");
```

Output on the Console window

```
"Enter the year that you would like to check the number
of days for each month"

Year= 1987

"Month Number:             "
"Number of days per month: "

1.  2.  3.  4.  5.  6.  7.  8.  9.  10. 11.  12.
31. 28. 31. 30. 31. 30. 31. 31. 30. 31. 30.  31.

"Would you like to repeat?"

Press "1" for YES or any key for NO: 1



"Enter the year that you would like to check the number
of days for each month"

Year= 1988

"Month Number:             "
"Number of days per month: "

1.  2.  3.  4.  5.  6.  7.  8.  9.  10. 11.  12.
31. 29. 31. 30. 31. 30. 31. 31. 30. 31. 30.  31.

"Would you like to repeat?"

Press "1" for YES or any key for NO: 2



"Thanks for using this application!  "
"************************************"
"Copyrighted (C) Claude Ziad El-Bayeh"
"************************************"
```

M x W x D + R = 366 days in a leap year (4)

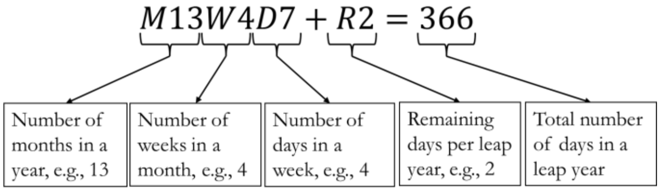

Figure 5. Example of annotating a calendar with the name M13W4D7+R2, which means there are 13 months a year, 4 weeks a month, 7 days a week, and 2 remaining days in a leap year.

M presents the number of months in a year (e.g., M = 12 months in a year). W shows the number of weeks in a month (e.g., W = 4 weeks in a month). D stands for the number of days in a week (e.g., D = 7 days in a week). R describes the number of remaining days that fill the gap between a perennial calendar and the actual number of days in a leap year (366). For example, calculate R if there are 12 months a year, 4 weeks a month, and 7 days a week. In this case, M=12, W=4, D=7. Hence,

M x W x D + R = 12 months/year x 4 weeks/month x 7 days/week + R = 366

⇒R = 366 – 12 x 4 x 7 = 30 remaining days per leap year

Based on the above-mentioned example, the number of remaining days per year is almost equal to one month for the Gregorian calendar. Therefore, the Gregorian calendar cannot be considered a good example of a perennial calendar. From this place, the real number of months in a year should be equal to 13 in the above case. An ideal perennial calendar is when the remaining number of days in a year will be equal to zero, hence R = 0. However, this is not possible for the Earth because the number of days in a year does not have an integer value, and it is equal almost to 365.2422. Therefore, it is necessary to rearrange the number of days, weeks, and months in order to minimize R. Thus, it becomes an optimization problem in which we need to recalculate the number of months, weeks, and days in a way to minimize R.

3.1 Optimization Model

As discussed previously, to minimize the number of remaining days in a year, an optimization model should be created. The objective function is described in Eq. (5), and the constraints are shown in Equations (6) to (10). Where, R_{min} and R_{max} describe the lower and upper bound of the number of remaining days in a perennial calendar. M_{min} and M_{max} are the lower and upper bound of the number of months per year. W_{min} and W_{max} represent the lower and upper bound of the number of weeks per month. D_{min} and D_{max} show the lower and upper bound of the number of days per week. It is obvious that the optimization problem is mixed-integer nonlinear programming in which M, W, D, and R should be integers. To solve the problem, the Mixed-Integer Genetic Algorithm (MIGA) is used in this paper.

Objective function:

Minimize $R = Y - M * W * D$ (5)

Subject to :

$$R_{Min} \leq Y - M * Y * D \leq R_{Max} \quad (6)$$

$$M_{Min} \leq M \leq M_{Max} \quad (7)$$

$$W_{Min} \leq W \leq W_{Max} \quad (8)$$

$$D_{Min} \leq D \leq D_{Max} \quad (9)$$

$$[r, M, W, D] \in \mathbb{N} \quad (10)$$

3.2 Optimization Algorithm

To solve the above problem, Algorithm 1 is proposed and written in MATLAB 2018b. The initial values (such as Mmin, Mmax, etc.) can be changed according to the needs of the user. Mixed Integer Genetic Algorithm (MIGA) is used as an optimization technique to solve the problem. The initial values of the input are stated in Table 4.

4. RESULTS AND DISCUSSIONS

4.1 Assumptions

After defining the optimization model and algorithm, it is necessary to present the assumptions that are considered in this paper. The optimization model requires the user to set the boundaries of the constraints. For this purpose, the limits are defined as follows:

- The remaining number of days in a year: Rmin=0 and Rmax=10. By increasing the range, more options appear to the user to choose the best calendar that fits his needs.
- The number of months in a year: Mmin=10 and Mmax=20. We do not want a number of months less than 10 because they become very long.
- Number of Weeks in a month: Wmin=0 and Wmax=20. We set the number of weeks flexible in order to get more options.
- Number of Days in a week: Dmin=5 and Dmax=8. A number less than 5 represents a too-short week, and a number greater than 8 is considered too long for a week.

4.2 Output results of the algorithm

Table 5 presents a selected list of options with their input and output results for the number of months, weeks, days, and remaining days per year for the proposed perennial calendars. The values can change when the boundaries of the constraints change.

Table 4. Input of the optimization model.

Input								
Y	**Rmin**	**Rmax**	**Mmin**	**Mmax**	**Wmin**	**Wmax**	**Dmin**	**Dmax**
366	0	10	10	20	0	20	5	8

Algorithm 1. Optimization model of the proposed original perennial calendar.

```
%% An Original Optimal Perennial Calendar

clc;clear;close all;%Clear all previous data on MATLAB


%% Optimization Model-------------------------------
for section1=1:1%Initial Values
    Y=366; %Number of days in a leap year
    Mmin=0; Mmax=20; %minimum and maximum number of
           months in a year
    Wmin=0; Wmax=20; %minimum and maximum number of
           Weeks in a Month
    Dmin=5; Dmax=8; %minimum and maximum number of
           Days in a Week
    Rmin=0; Rmax=10; %minimum and maximum number of
           remaining Days in a Year
End


for section1=1:1%Optimization Model
    %Decision variable: X, X(1)=Month, X(2)=Week,
      X(3)=Day
    OF=@(X)(Y-X(1).*X(2).*X(3)); %Objective Function

    %Constraints of the Form A*x<=B
    A=[1 0 0 ; 0 1 0 ; 0 0 1]; B=[Mmax, Wmax, Dmax]';

    %Constraints of the Form Aeq*x=Beq
    Aeq=[]; Beq=[];

    %Constraints of the Form lb<=x<=ub
    LB=[Mmin Wmin Dmin]'; %Lower Bound
    UB=[Mmax Wmax Dmax]'; %Upper Bound

    X0=zeros(3,1);%Starting point

    %Solution of the Optimization
    nvar=3; %Number of studied variables
    IntCon=[1,2,3]; %Variable that should be integer

    [X,Value,exitflag,output]=ga(OF,nvar,A,B,Aeq,Beq,
      LB, UB,@C_Matrix,IntCon);

    X %Show the number of Variable

    R=Value %Show the remaining number of days

    MWD=X(1).*X(2).*X(3) %Show total number of days in
          a year except the remaining days

    fprintf('M=%2.0f  , W=%2.0f, D=%2.0f, R= %2.0f ,
          MWD= %2.0f \n',X,R,MWD)
end


function [C,Ceq] = C_Matrix(X)
    Y=366;
    Rmin=0; Rmax=10;
    C(1)= X(1).*X(2).*X(3)-Y+Rmin;
    C(2)= Y-X(1).*X(2).*X(3)-Rmax;
    Ceq=[];
end
```

Table 5. Input and Output Results of the Optimization Model.

	Input								Output							
Options	**Rmin**	**Rmax**	**Mmin**	**Mmax**	**Wmin**	**Wmax**	**Dmin**	**Dmax**	**M**	**W**	**D**	**R**	**MWD**	**Nb of weeks in a year**	**Perfect Calendar**	**Semi-Perfect Calendar**
1	0	10	10	20	0	20	5	8	10	6	6	6	360	**60**	**Yes**	-
2	0	10	10	20	0	20	5	8	12	6	5	6	360	72	No	Yes
3	0	10	10	20	0	20	5	8	12	5	6	6	360	**60**	**Yes**	-
4	0	10	10	20	0	20	5	8	12	3	10	6	360	36	No	Yes
5	0	10	10	20	0	20	5	8	13	4	7	2	364	52	No	No
6	0	10	10	20	0	20	5	8	15	4	6	6	360	**60**	**Yes**	-
7	0	10	10	20	0	20	5	8	15	3	8	6	360	45	No	No
8	0	10	10	20	0	20	5	8	18	4	5	6	360	72	No	Yes
9	0	10	10	20	0	20	5	8	20	3	6	6	360	**60**	**Yes**	-

A calendar that has 13 months, such as some of the proposed Optimal Perennial Calendars in this paper, has a prime number “13” which cannot be divided by 2, nor by 3 neither by 4. Therefore, it becomes difficult to categorize activities based on a biannually, triannually, or quarterly basis. In order to solve the problem, dividing the year into many intervals can be done on a weekly basis in which the total number of weeks in a 13 months calendar system is equal to 52 (13x4).

In this paper, a perfect calendar is defined as a calendar which can be divided into many equal intervals (particularly 2 (biannually), 3 (triannually), 4 (quarterly), 5 (quinannually), and 6 (sexannually) with the exact number of weeks in each interval. A semi-perfect calendar is defined as a calendar that can satisfy at least 4 of the previously mentioned intervals (2, 3, 4, 5, and 6), as presented in Table 6.

Table 6. Example of dividing a year into intervals with the same number of weeks for different perennial calendars.

Proposed optimal perennial calendar systems		**M12W3D10+R6**	**M15W3D8+R6**	**M15W3D8+R6**	**M13W4D7+R2**	**M12W5D6+R6**	**M10W6D6+R6**	**M12W6D5+R6**	**M18W4D5+R6**
Number of Weeks		**36**	**45**	**45**	**52**	**60**	**60**	**72**	**72**
Interval per year	2	18	22.50	22.50	26	30	30	36	36
	3	12	15	15	17.33	20	20	24	24
	4	9	11.25	11.25	13	15	15	18	18
	5	7.20	9	9	10.40	12	12	14.40	14.40
	6	6	7.50	7.50	8.67	10	10	12	12
Perfect Calendar		**No**	No	No	No	**Yes**	**Yes**	No	No
Semi-Perfect Calendar		**Yes**	No	No	No	-	-	**Yes**	**Yes**

4.3 Case Study of a Calendar with 13 Months, 4 Weeks and 7 days (M13W4D7+R2)

In this paper, only the perennial calendar “M13W4D7+R2” (option 5) is discussed, while others can be interpreted in the same way. Table 7 presents the proposed perennial calendar "M13W4D7+R2” based on some new rules, as stated below:

- One year has 13 months with an exact number of days and weeks. No days are added to any month nor to any week. Hence, the drawback (a) mentioned in section 1.3 is resolved,
- Each month has exactly 4 weeks,
- Each week has exactly 7 days. Therefore, the total number of days in a year becomes equal to 364 (7 days x 4 weeks x 13 months),
- A new month is added to the list, which is called “Month Zero”, in which it contains the remaining days (Year-day and the Leap-day). The reason for adding this month is to separate the remaining days from the normal days, which is not the case with IFC. In addition, it respects the international standard ISO 8601, in which the dates are expressed. For example, 2020-00-01 is the Year-day, 2020-00-02 is the leap-day in a leap year, 2020-01-01 is the first official day of the year 2020, which is Monday, etc. Therefore, there is a consistency in numbering the days, dates, and their expressions,
- We do not celebrate the end of a year as other existing calendars do, such as the GC, JC, and IFC. On the contrary, we celebrate the beginning of a new year. That is why Month Zero is added at the beginning, which represents a new start and a happy month in our lives. This method has a positive impact on the psychology of the people in which the end is not important as the beginning of a new thing in their life,
- Friday will never occur on the 13th of any month. Therefore, some people who feel pessimistic about this date will be satisfied with the new calendar. Hence, the problem (e) in section 1.3 is solved,
- The Year-Day and Leap-Day only belong to the “Month Zero”. Therefore, months still have the same number of days and will never change. Therefore, the problem (d) in section 1.3 is solved,
- A leap year has 366 days, and its occurrence follows the Gregorian rules,
- Each week starts on Monday and ends on Sunday, which agrees with the international standard ISO 8601. Therefore, the problems (c) and (f) in section 1.3 are addressed,
- Each month starts on Monday and ends on a Sunday,
- Every year starts on Monday and ends on Sunday. Therefore, Month Zero is considered as a fictive month with a maximum of 2 days, which are feast days that celebrate the beginning of a new year.
- For business purposes, instead of dividing the year into quarters or triannuals, it is recommended to consider weeks that give more accurate results. For example, if we want to divide a year into 4 quarters, in the proposed

calendar, each quarter is exactly 13 weeks. For a triannual year, 17 weeks are considered for the first two triannually -based year, and 18 weeks are considered for the third period. Therefore, problem (b) mentioned in section 1.3 is solved.

Table 7. Proposed perennial calendar M13W4D7+R2.

The proposed Perennial Calendar M13W4D7+R2

Year: Any year has the same sequence of days and dates

Month Zero	
Year-day	Leap-day
1	2

# of Working Days:	260
# of Off Days:	105

Month 1 (January)						
M	T	W	T	F	S	S
1	2	3	4	5	6	7
8	9	10	11	12	13	14
15	16	17	18	19	20	21
22	23	24	25	26	27	28

Month 2 (February)						
M	T	W	T	F	S	S
1	2	3	4	5	6	7
8	9	10	11	12	13	14
15	16	17	18	19	20	21
22	23	24	25	26	27	28

Month 3 (March)						
M	T	W	T	F	S	S
1	2	3	4	5	6	7
8	9	10	11	12	13	14
15	16	17	18	19	20	21
22	23	24	25	26	27	28

Month 4 (April)						
M	T	W	T	F	S	S
1	2	3	4	5	6	7
8	9	10	11	12	13	14
15	16	17	18	19	20	21
22	23	24	25	26	27	28

Month 5 (May)						
M	T	W	T	F	S	S
1	2	3	4	5	6	7
8	9	10	11	12	13	14
15	16	17	18	19	20	21
22	23	24	25	26	27	28

Month 6 (June)						
M	T	W	T	F	S	S
1	2	3	4	5	6	7
8	9	10	11	12	13	14
15	16	17	18	19	20	21
22	23	24	25	26	27	28

Month 7 (July)						
M	T	W	T	F	S	S
1	2	3	4	5	6	7
8	9	10	11	12	13	14
15	16	17	18	19	20	21
22	23	24	25	26	27	28

Month 8 (August)						
M	T	W	T	F	S	S
1	2	3	4	5	6	7
8	9	10	11	12	13	14
15	16	17	18	19	20	21
22	23	24	25	26	27	28

Month 9 (September)						
M	T	W	T	F	S	S
1	2	3	4	5	6	7
8	9	10	11	12	13	14
15	16	17	18	19	20	21
22	23	24	25	26	27	28

Month 10 (October)						
M	T	W	T	F	S	S
1	2	3	4	5	6	7
8	9	10	11	12	13	14
15	16	17	18	19	20	21
22	23	24	25	26	27	28

Month 11 (November)						
M	T	W	T	F	S	S
1	2	3	4	5	6	7
8	9	10	11	12	13	14
15	16	17	18	19	20	21
22	23	24	25	26	27	28

Month 12 (December)						
M	T	W	T	F	S	S
1	2	3	4	5	6	7
8	9	10	11	12	13	14
15	16	17	18	19	20	21
22	23	24	25	26	27	28

Month 13 (Undecember)						
M	T	W	T	F	S	S
1	2	3	4	5	6	7
8	9	10	11	12	13	14
15	16	17	18	19	20	21
22	23	24	25	26	27	28

Based on Table 7, it is clear that the proposed Calendar has a more systematic organization of days and months in a year compared to the Gregorian calendar. The first day of a month always starts on Monday, and the last day of each month is always Sunday. Therefore, counting days becomes an easy task, and there is no need for complex algorithms to predict the days and dates in previous years. The days and dates in the proposed Calendar have strong and correlated relationships, which can be described by simple mathematical equations as in Eq.(11).

$$\begin{cases} Monday = 1 + 7(w-1) \\ Tuesday = 2 + 7(w-1) \\ Wednesday = 3 + 7(w-1) \\ Thursday = 4 + 7(w-1) \\ Friday = 5 + 7(w-1) \\ Saturday = 6 + 7(w-1) \\ Sunday = 7 + 7(w-1) \\ Yearday = 365 \\ Leap\ day = 366\ (in\ a\ leap\ year) \end{cases} \tag{11}$$

$$Where\ w\ is\ the\ week\ number\ in\ a \begin{cases} month: w \in [1,4] \\ year: w \in [1,52] \end{cases}$$

As an example, calculate the date of Monday in the third week of a month.

Answer: Monday $= 1 + 7(3-1) = 15$

March						
Mon	Tue	Wed	Thu	Fri	Sat	Sun
1	2	3	4	5	6	7
8	9	10	11	12	13	14
15	16	17	18	19	20	21
22	23	24	25	26	27	28

Another example, calculate the day number of Wednesday located on the 36th week of the year.

Answer: Wednesday $= 3 + 7(w-1) = 3 + 7(36-1) = 248$

July						
Mon	Tue	Wed	Thu	Fri	Sat	Sun
169	170	171	172	173	174	175
176	177	178	179	180	181	182
183	184	185	186	187	188	189
190	191	192	193	194	195	196

August						
Mon	Tue	Wed	Thu	Fri	Sat	Sun
197	198	199	200	201	202	203
204	205	206	207	208	209	210
211	212	213	214	215	216	217
218	219	220	221	222	223	224

September						
Mon	Tue	Wed	Thu	Fri	Sat	Sun
225	226	227	228	229	230	231
232	233	234	235	236	237	238
239	240	241	242	243	244	245
246	247	248	249	250	251	252

October						
Mon	Tue	Wed	Thu	Fri	Sat	Sun
253	254	255	256	257	258	259
260	261	262	263	264	265	266
267	268	269	270	271	272	273
274	275	276	277	278	279	280

4.4 Comparison between the proposed calendar and the Gregorian calendar

In this subsection, a comparison between the proposed and Gregorian calendars is presented. Table 8 shows both calendars, in which it is obvious that the proposed one is much easier to memorize because all months look the same. A more detailed comparison is presented in Table 9.

Table 8: Comparison between the proposed and Gregorian calendars.

The proposed Perennial Calendar M13W4D7+R2

Year: Any year has the same sequence of days and dates

Month Zero

Year-day	Leap-day
1	2

Month 1 (January)

M	T	W	T	F	S	S
1	2	3	4	5	6	7
8	9	10	11	12	13	14
15	16	17	18	19	20	21
22	23	24	25	26	27	28

Month 2 (February)

M	T	W	T	F	S	S
1	2	3	4	5	6	7
8	9	10	11	12	13	14
15	16	17	18	19	20	21
22	23	24	25	26	27	28

Month 3 (March)

M	T	W	T	F	S	S
1	2	3	4	5	6	7
8	9	10	11	12	13	14
15	16	17	18	19	20	21
22	23	24	25	26	27	28

Month 4 (April)

M	T	W	T	F	S	S
1	2	3	4	5	6	7
8	9	10	11	12	13	14
15	16	17	18	19	20	21
22	23	24	25	26	27	28

Month 5 (May)

M	T	W	T	F	S	S
1	2	3	4	5	6	7
8	9	10	11	12	13	14
15	16	17	18	19	20	21
22	23	24	25	26	27	28

Month 6 (June)

M	T	W	T	F	S	S
1	2	3	4	5	6	7
8	9	10	11	12	13	14
15	16	17	18	19	20	21
22	23	24	25	26	27	28

Month 7 (July)

M	T	W	T	F	S	S
1	2	3	4	5	6	7
8	9	10	11	12	13	14
15	16	17	18	19	20	21
22	23	24	25	26	27	28

Month 8 (August)

M	T	W	T	F	S	S
1	2	3	4	5	6	7
8	9	10	11	12	13	14
15	16	17	18	19	20	21
22	23	24	25	26	27	28

Month 9 (September)

M	T	W	T	F	S	S
1	2	3	4	5	6	7
8	9	10	11	12	13	14
15	16	17	18	19	20	21
22	23	24	25	26	27	28

Month 10 (October)

M	T	W	T	F	S	S
1	2	3	4	5	6	7
8	9	10	11	12	13	14
15	16	17	18	19	20	21
22	23	24	25	26	27	28

Month 11 (November)

M	T	W	T	F	S	S
1	2	3	4	5	6	7
8	9	10	11	12	13	14
15	16	17	18	19	20	21
22	23	24	25	26	27	28

Month 12 (December)

M	T	W	T	F	S	S
1	2	3	4	5	6	7
8	9	10	11	12	13	14
15	16	17	18	19	20	21
22	23	24	25	26	27	28

Month 13 (Undecember)

M	T	W	T	F	S	S
1	2	3	4	5	6	7
8	9	10	11	12	13	14
15	16	17	18	19	20	21
22	23	24	25	26	27	28

Gregorian Calendar

Only for the year 2020, the dispalcement of dates and days change

January 2020

S	M	T	W	T	F	S
			1	2	3	4
5	6	7	8	9	10	11
12	13	14	15	16	17	18
19	20	21	22	23	24	25
26	27	28	29	30	31	

February 2020

S	M	T	W	T	F	S
						1
2	3	4	5	6	7	8
9	10	11	12	13	14	15
16	17	18	19	20	21	22
23	24	25	26	27	28	29

March 2020

S	M	T	W	T	F	S
1	2	3	4	5	6	7
8	9	10	11	12	13	14
15	16	17	18	19	20	21
22	23	24	25	26	27	28
29	30	31				

April 2020

S	M	T	W	T	F	S
			1	2	3	4
5	6	7	8	9	10	11
12	13	14	15	16	17	18
19	20	21	22	23	24	25
26	27	28	29	30		

May 2020

S	M	T	W	T	F	S
					1	2
3	4	5	6	7	8	9
10	11	12	13	14	15	16
17	18	19	20	21	22	23
24	25	26	27	28	29	30
31						

June 2020

S	M	T	W	T	F	S
	1	2	3	4	5	6
7	8	9	10	11	12	13
14	15	16	17	18	19	20
21	22	23	24	25	26	27
28	29	30				

July 2020

S	M	T	W	T	F	S
			1	2	3	4
5	6	7	8	9	10	11
12	13	14	15	16	17	18
19	20	21	22	23	24	25
26	27	28	29	30	31	

August 2020

S	M	T	W	T	F	S
						1
2	3	4	5	6	7	8
9	10	11	12	13	14	15
16	17	18	19	20	21	22
23	24	25	26	27	28	29
30	31					

September 2020

S	M	T	W	T	F	S
		1	2	3	4	5
6	7	8	9	10	11	12
13	14	15	16	17	18	19
20	21	22	23	24	25	26
27	28	29	30			

October 2020

S	M	T	W	T	F	S
				1	2	3
4	5	6	7	8	9	10
11	12	13	14	15	16	17
18	19	20	21	22	23	24
25	26	27	28	29	30	31

November 2020

S	M	T	W	T	F	S
1	2	3	4	5	6	7
8	9	10	11	12	13	14
15	16	17	18	19	20	21
22	23	24	25	26	27	28
29	30					

December 2020

S	M	T	W	T	F	S
		1	2	3	4	5
6	7	8	9	10	11	12
13	14	15	16	17	18	19
20	21	22	23	24	25	26
27	28	29	30	31		

Table 9: Comparison between three calendars, the proposed one (M13W4D7+R2), Gregorian, and IFC.

Aspects	Description	Proposed Calendar	GC	IFC
Technical	Number of weekends in a year	**Up to 106**	Up to 104	**Up to 106**
	Complexity of the system	**Very easy**	Complex	Easy
	Computation time	**Very low**	Very high [26]	Low
	Reduce wasted time to check days and dates on a calendar	**Very low**	Very high	Low
	Do we need a Calendar to check the dates	**No**	Yes	**No**
	Considered as Perennial Calendar	**Yes**	No	**Yes**
	The date of days does not change (e.g., the 17th always falls on a Tuesday)	**Yes**	No	**Yes**
	Calendar respects international standards	**Yes**	No	No
Economic	Number of payable months	**13**	12	**13**
	Easy scheduling for institutions and industries with extended production cycles	**Yes**	No	**Yes**
	Accurate statistical comparisons by months, since all months have exactly the same number of business days and weekends	**Yes**	No	**Yes**
	Possibility of error in printing the calendar and calculating the dates	**No**	Yes [27]	**No**
	Can be considered as a financial calendar in which years can be divided into quarters, triannuals, and biannuals	**Yes (based on weeks instead of months)**	**Yes**	No
Environ-mental	Eco-friendly	**Yes**	No	**Yes**
	Reduce the number of printed hard-copies	**Yes**	No	**Yes**
	Reduce pollution and waste from printing the calendars	**Yes**	No	**Yes**
	Reduce energy consumption	**Yes**	No	**Yes**
Indivi-dual	Better organization of personal life	**Yes**	No	**Yes**
	Accurate appointments and events	**Yes**	No	**Yes**
Social	Movable holidays celebrated on the *n*th certain weekday of a month, (e.g., Thanksgiving Day), would be able to have a fixed date while keeping their traditional weekday	**Yes**	No	**Yes**
	Better organization of social activities	**Yes**	No	**Yes**
	Less conflict because of missing some events, meetings, and appointments	**Yes**	No	**Yes**

4.5 Other proposed Calendars

In the previous subsection, the proposed calendar "M13W4D7+R2" is discussed. However, Table 5 shows other possible solutions, in which some of them will be presented briefly in this subsection. In Tables 10 to 13, only 4 calendars are presented, which come from Table 5. The yellow boxes represent the weekends and the day offs, and the white boxes are for the working days.

Table 10. Proposed calendar: M12W5D6+R6.

The proposed Calendar M12W5D6+R6

Year: Any year has the same sequence of days and dates

Month 01

D1	D2	D3	D4	D5	D6
1	2	3	4	5	6
7	8	9	10	11	12
13	14	15	16	17	18
19	20	21	22	23	24
25	26	27	28	29	30

Month 02

D1	D2	D3	D4	D5	D6
1	2	3	4	5	6
7	8	9	10	11	12
13	14	15	16	17	18
19	20	21	22	23	24
25	26	27	28	29	30

Month 03

D1	D2	D3	D4	D5	D6
1	2	3	4	5	6
7	8	9	10	11	12
13	14	15	16	17	18
19	20	21	22	23	24
25	26	27	28	29	30

Month 04

D1	D2	D3	D4	D5	D6
1	2	3	4	5	6
7	8	9	10	11	12
13	14	15	16	17	18
19	20	21	22	23	24
25	26	27	28	29	30

Month 05

D1	D2	D3	D4	D5	D6
1	2	3	4	5	6
7	8	9	10	11	12
13	14	15	16	17	18
19	20	21	22	23	24
25	26	27	28	29	30

Month 06

D1	D2	D3	D4	D5	D6
1	2	3	4	5	6
7	8	9	10	11	12
13	14	15	16	17	18
19	20	21	22	23	24
25	26	27	28	29	30

Month 07

D1	D2	D3	D4	D5	D6
1	2	3	4	5	6
7	8	9	10	11	12
13	14	15	16	17	18
19	20	21	22	23	24
25	26	27	28	29	30

Month 08

D1	D2	D3	D4	D5	D6
1	2	3	4	5	6
7	8	9	10	11	12
13	14	15	16	17	18
19	20	21	22	23	24
25	26	27	28	29	30

Month 09

D1	D2	D3	D4	D5	D6
1	2	3	4	5	6
7	8	9	10	11	12
13	14	15	16	17	18
19	20	21	22	23	24
25	26	27	28	29	30

Month 10

D1	D2	D3	D4	D5	D6
1	2	3	4	5	6
7	8	9	10	11	12
13	14	15	16	17	18
19	20	21	22	23	24
25	26	27	28	29	30

Month 11

D1	D2	D3	D4	D5	D6
1	2	3	4	5	6
7	8	9	10	11	12
13	14	15	16	17	18
19	20	21	22	23	24
25	26	27	28	29	30

Month 12

D1	D2	D3	D4	D5	D6
1	2	3	4	5	6
7	8	9	10	11	12
13	14	15	16	17	18
19	20	21	22	23	24
25	26	27	28	29	30

Month 13 (Year-Month)

YD1	YD2	YD3	YD4	YD5	YD6
1	2	3	4	5	6 ← For the day 366 in a leap year

For days 361 to 365

# of Working Days: 264

# of Off Days: 102

This calendar has 12 official months. Each month has 5 weeks of 6 days each. At the end of the year, an additional Month is added with only 5 days (+1 leap day in a leap year). These days are called Yeardays, in which they are different from the normal days, and can be considered as holidays or day off for employees.

Table 11. Proposed calendar: M12W6D5+R6.

The proposed Calendar M12W6D5+R6

Year: Any year has the same sequence of days and dates

Month 01

D1	D2	D3	D4	D5
1	2	3	4	5
6	7	8	9	10
11	12	13	14	15
16	17	18	19	20
21	22	23	24	25
26	27	28	29	30

Month 02

D1	D2	D3	D4	D5
1	2	3	4	5
6	7	8	9	10
11	12	13	14	15
16	17	18	19	20
21	22	23	24	25
26	27	28	29	30

Month 03

D1	D2	D3	D4	D5
1	2	3	4	5
6	7	8	9	10
11	12	13	14	15
16	17	18	19	20
21	22	23	24	25
26	27	28	29	30

Month 04

D1	D2	D3	D4	D5
1	2	3	4	5
6	7	8	9	10
11	12	13	14	15
16	17	18	19	20
21	22	23	24	25
26	27	28	29	30

Month 05

D1	D2	D3	D4	D5
1	2	3	4	5
6	7	8	9	10
11	12	13	14	15
16	17	18	19	20
21	22	23	24	25
26	27	28	29	30

Month 06

D1	D2	D3	D4	D5
1	2	3	4	5
6	7	8	9	10
11	12	13	14	15
16	17	18	19	20
21	22	23	24	25
26	27	28	29	30

Month 07

D1	D2	D3	D4	D5
1	2	3	4	5
6	7	8	9	10
11	12	13	14	15
16	17	18	19	20
21	22	23	24	25
26	27	28	29	30

Month 08

D1	D2	D3	D4	D5
1	2	3	4	5
6	7	8	9	10
11	12	13	14	15
16	17	18	19	20
21	22	23	24	25
26	27	28	29	30

Month 09

D1	D2	D3	D4	D5
1	2	3	4	5
6	7	8	9	10
11	12	13	14	15
16	17	18	19	20
21	22	23	24	25
26	27	28	29	30

Month 10

D1	D2	D3	D4	D5
1	2	3	4	5
6	7	8	9	10
11	12	13	14	15
16	17	18	19	20
21	22	23	24	25
26	27	28	29	30

Month 11

D1	D2	D3	D4	D5
1	2	3	4	5
6	7	8	9	10
11	12	13	14	15
16	17	18	19	20
21	22	23	24	25
26	27	28	29	30

Month 12

D1	D2	D3	D4	D5
1	2	3	4	5
6	7	8	9	10
11	12	13	14	15
16	17	18	19	20
21	22	23	24	25
26	27	28	29	30

Month 13 (Year-Month)

YD1	YD2	YD3	YD4	YD5	YD6
1	2	3	4	5	6 ← For the day 366 in a leap year

For day 365

# of Working Days: 264

# of Off Days: 102

This calendar has 12 official months. Each month has 6 weeks of 5 days each. At the end of the year, an additional Month is added with only 5 days (+1 leap day in a leap year). These days are called Yeardays, in which they are different from the normal days, and can be considered as holidays or day off for employees.

Table 12. Proposed calendar: M10W6D6+R6.

The proposed Calendar M10W6D6+R6

Year: Any year has the same sequence of days and dates

Month 01

D1	D2	D3	D4	D5	D6
1	2	3	4	5	6
7	8	9	10	11	12
13	14	15	16	17	18
19	20	21	22	23	24
25	26	27	28	29	30
31	32	33	34	35	36

Month 02

D1	D2	D3	D4	D5	D6
1	2	3	4	5	6
7	8	9	10	11	12
13	14	15	16	17	18
19	20	21	22	23	24
25	26	27	28	29	30
31	32	33	34	35	36

Month 03

D1	D2	D3	D4	D5	D6
1	2	3	4	5	6
7	8	9	10	11	12
13	14	15	16	17	18
19	20	21	22	23	24
25	26	27	28	29	30
31	32	33	34	35	36

Month 04

D1	D2	D3	D4	D5	D6
1	2	3	4	5	6
7	8	9	10	11	12
13	14	15	16	17	18
19	20	21	22	23	24
25	26	27	28	29	30
31	32	33	34	35	36

Month 05

D1	D2	D3	D4	D5	D6
1	2	3	4	5	6
7	8	9	10	11	12
13	14	15	16	17	18
19	20	21	22	23	24
25	26	27	28	29	30
31	32	33	34	35	36

Month 06

D1	D2	D3	D4	D5	D6
1	2	3	4	5	6
7	8	9	10	11	12
13	14	15	16	17	18
19	20	21	22	23	24
25	26	27	28	29	30
31	32	33	34	35	36

Month 07

D1	D2	D3	D4	D5	D6
1	2	3	4	5	6
7	8	9	10	11	12
13	14	15	16	17	18
19	20	21	22	23	24
25	26	27	28	29	30
31	32	33	34	35	36

Month 08

D1	D2	D3	D4	D5	D6
1	2	3	4	5	6
7	8	9	10	11	12
13	14	15	16	17	18
19	20	21	22	23	24
25	26	27	28	29	30
31	32	33	34	35	36

Month 09

D1	D2	D3	D4	D5	D6
1	2	3	4	5	6
7	8	9	10	11	12
13	14	15	16	17	18
19	20	21	22	23	24
25	26	27	28	29	30
31	32	33	34	35	36

Month 10

D1	D2	D3	D4	D5	D6
1	2	3	4	5	6
7	8	9	10	11	12
13	14	15	16	17	18
19	20	21	22	23	24
25	26	27	28	29	30
31	32	33	34	35	36

Month 11 (Year-Month)

YD1	YD2	YD3	YD4	YD5	YD6
1	2	3	4	5	6 ← For the day 366 in a leap year

For days 361 to 365

# of Working Days: 260

# of Off Days: 106

This calendar has 10 official months. Each month has 6 weeks of 6 days each. At the end of the year, an additional Month is added with only 5 days (+1 leap day in a leap year). These days are called Yeardays, in which they are different from the normal days, and can be considered as holidays or day off for employees.

Table13. Proposed calendar: M15W3D8+R6.

The proposed Calendar M15W3D8+R6

Year: Any year has the same sequence of days and dates

Month 01

D1	D2	D3	D4	D5	D6	D7	D8
1	2	3	4	5	6	7	8
9	10	11	12	13	14	15	16
17	18	19	20	21	22	23	24

Month 02

D1	D2	D3	D4	D5	D6	D7	D8
1	2	3	4	5	6	7	8
9	10	11	12	13	14	15	16
17	18	19	20	21	22	23	24

Month 03

D1	D2	D3	D4	D5	D6	D7	D8
1	2	3	4	5	6	7	8
9	10	11	12	13	14	15	16
17	18	19	20	21	22	23	24

Month 04

D1	D2	D3	D4	D5	D6	D7	D8
1	2	3	4	5	6	7	8
9	10	11	12	13	14	15	16
17	18	19	20	21	22	23	24

Month 05

D1	D2	D3	D4	D5	D6	D7	D8
1	2	3	4	5	6	7	8
9	10	11	12	13	14	15	16
17	18	19	20	21	22	23	24

Month 06

D1	D2	D3	D4	D5	D6	D7	D8
1	2	3	4	5	6	7	8
9	10	11	12	13	14	15	16
17	18	19	20	21	22	23	24

Month 07

D1	D2	D3	D4	D5	D6	D7	D8
1	2	3	4	5	6	7	8
9	10	11	12	13	14	15	16
17	18	19	20	21	22	23	24

Month 08

D1	D2	D3	D4	D5	D6	D7	D8
1	2	3	4	5	6	7	8
9	10	11	12	13	14	15	16
17	18	19	20	21	22	23	24

Month 09

D1	D2	D3	D4	D5	D6	D7	D8
1	2	3	4	5	6	7	8
9	10	11	12	13	14	15	16
17	18	19	20	21	22	23	24

Month 10

D1	D2	D3	D4	D5	D6	D7	D8
1	2	3	4	5	6	7	8
9	10	11	12	13	14	15	16
17	18	19	20	21	22	23	24

Month 11

D1	D2	D3	D4	D5	D6	D7	D8
1	2	3	4	5	6	7	8
9	10	11	12	13	14	15	16
17	18	19	20	21	22	23	24

Month 12

D1	D2	D3	D4	D5	D6	D7	D8
1	2	3	4	5	6	7	8
9	10	11	12	13	14	15	16
17	18	19	20	21	22	23	24

Month 13

D1	D2	D3	D4	D5	D6	D7	D8
1	2	3	4	5	6	7	8
9	10	11	12	13	14	15	16
17	18	19	20	21	22	23	24

Month 14

D1	D2	D3	D4	D5	D6	D7	D8
1	2	3	4	5	6	7	8
9	10	11	12	13	14	15	16
17	18	19	20	21	22	23	24

Month 15

D1	D2	D3	D4	D5	D6	D7	D8
1	2	3	4	5	6	7	8
9	10	11	12	13	14	15	16
17	18	19	20	21	22	23	24

Month 11 (Year-Month)

YD1	YD2	YD3	YD4	YD5	YD6
1	2	3	4	5	6 ←For the day 366 in a leap year

For days 361 to 365

# of Working Days: 255

# of Off Days: 111

This calendar has 15 official months. Each month has 3 weeks of 8 days each. At the end of the year, an additional Month is added with only 5 days (+1 leap day in a leap year). These days are called Yeardays that they are different from the normal days, and can be considered as holidays or day off for employees

4.6 Impact on the Environment and Energy Demand

The rotation of the Earth around the Sun takes almost 365.2422 days which is neither an even number nor an integer and cannot be divided into equal intervals. Therefore, it was challenging to create a user-friendly and easy to memorize calendar in which the number of days, weeks, and months are distributed equally along the year. Gregorian calendar was one of many attempts to create an accurate calendar that reduces the calculation error in counting the number of days on a long period, as mentioned in Table 1. Despite the accuracy of the Gregorian calendar, it has lots of drawbacks. It is not a user-friendly calendar, and it is not easy to memorize the days and their corresponding dates. Therefore, it was necessary to print out the calendar on paper, which will increase the pollution and the emission of Green House Gases (GHG) such as CO_2. In addition, lots of energy is consumed to produce and distribute these paper-based calendars. In modern times, computers, cell phones, and smartwatches are mostly used to check the days and dates and save events. They do not consume paper; however, they still consume lots of energy, as will be calculated in the following subsections.

4.6.1 Impact on the energy demand

In order to proceed in the calculation, it is important to select the most pertinent data set for the problem. In this subsection, we intend to collect data of mobile and computer users in order to calculate the impact of using digital calendars on total energy consumption worldwide. In other meaning, we will calculate the wasted energy by checking the dates and days using digital calendars. Input data are presented as follows:

- Current world population 7.9 billion people (2021),
- Number of mobile phone users: 5.27 billion [28],
- Number of computer users: 2 billion [29],
- Average time spent to check the days and dates on the calendar per user per day: 5 minutes,
- Efficiency from power generation to consumption: 0.88 considering losses on transmission/distribution lines,
- Average energy consumption of a mobile per day: 12Wh,
- Average power consumption of a mobile: 1.8W average,
- Charging efficiency: 0.9,
- Average power consumption of a computer: 60W (considering desktops, and laptops).

Table 14. Average computer energy consumption [30].

Computer Type	Energy Consumption
Desktop Computer	60-250 Watts
Computer with Active Screen Saver	60-250 Watts
Computer on Sleep or Standby	1-6 Watts
Laptop	15-45 Watts

Table 15 presents the calculation made to find out the wasted energy to check the days and dates on a calendar for all users across the globe per year using computers and mobile phones. It was found that almost 293 GWh/year are wasted just to check the Gregorian calendar, while it is about 23.4 GWh/year for the proposed Optimal Perennial Calendar (M13W4D7+R2) in the worst-case scenario. Therefore, the proposed optimal perennial calendar system has reduced the energy demand by at least 12.5 times compared to the Gregorian calendar.

Table 15. Wasted energy to check dates & days using GC and OPC (M13W4D7+R2).

Description	**Value**		**Unit**	**Equation**
Population	7.90E+09		-	A
Number of mobile users	5.27E+09		-	B
Number of computer users	2.00E+09		-	C
Average time spent to check the days and dates on the calendar per user per day	3.47E-03	2.78E-04	[hour/day]	D=(5/60)min / 24h
Mobile phone	**GC**	**OPC**	**Unit**	**Equation**
Average energy consumption of a mobile per day	12	12	[Wh/day]	E
Average energy consumption of a mobile per day from the generation side (considering losses of the charger (10%), distribution and transmission lines (12%))	15.152	15.152	[Wh/day]	F=E/(0.9*0.88)
Average energy consumption of a mobile per day to check the days and dates on the calendar from the generation side (considering losses of the charger (10%), distribution and transmission lines (12%))	0.0526	0.0042	[Wh/day]	G=F*D
Average energy consumption of all mobile phones for all users to check the days and dates on the calendar from the generation side	277,252	22,180	[kWh/day]	H=G*B/1000
	277.252	22.180	[MWh/day]	I=H/1000
	101.197	**8.096**	**[GWh/year]**	**J=I*365/1000**
Computer	**GC**	**OPC**	**Unit**	**Equation**
Average power consumption of a computer/laptop	60	60	[W]	K
Average energy consumption of a computer per day to check the days and dates on the calendar	0.2083	0.0167	[Wh/day]	L=K*D
Average energy consumption of a computer per day to check the days and dates on the calendar from the generation side	0.2630	0.0210	[Wh/day]	M=L/(0.9*0.88)
Average energy consumption of all computers for all users to check the days and dates on the calendar from the generation side	526,094	42,088	[kWh/day]	N=M*C/1000
	526.094	42.088	[MWh/day]	O=N/1000
	192.024	**15.362**	**[GWh/year]**	**P=O*365/1000**
Total energy demand to check the calendar per year for all users	**293.221**	**23.458**	**[GWh/year]**	**Q=P+J**

4.6.2 Impact on the CO_2 emission and pollution

The production of paper-based calendars every year does not only increase the energy waste but also increases the CO_2 emission and the waste, as presented in Table 16. It can be remarked that the CO_2 emission by producing only paper-based calendars may exceed 3.8 million tons per year and yield about 1.9 million tons of waste. Of course, we did not consider the pollution from the power plant sources since we assume that the energy production comes from renewable energy sources such as photovoltaics and wind turbines, using storage systems such as batteries. In the case when fuel-based power plants are used, the figures could be tripled since the average efficiency of most of the fuel-based power plants does not exceed 33%.

Table16. CO_2 emission and waste production using GC and OPC(M13W4D7+R2).

Calendar	GC	OPC		
Description	**Value**	**Value**	**Unit**	**Equation**
Population	7.90E+09	7.90E+09	-	A
Sold calendars per year (including wall calendars, and paper calendars)	1.90E+09	1.90E+09	-	B
Average number of sheets per calendar	200	0.1	-	C
Number of sheets produced each year to create paper-based calendars	3.80E+11	1.90E+08	sheet/year	D=C*B
CO2 emission per paper sheet	5	5	g of CO2/sheet	E
CO2 emission per printed paper sheet	10	10	g of CO2/sheet	F
Total CO2 emission per year	3.80E+09	1.90E+06	kg/year	G=D*F/1000
	3.80E+06	**1.90E+03**	**Ton/year**	**H=G/1000**
CO2 reduction ratio (GC/OPC)		**2000**	**Ton/year**	H(GC)/H(OPC)
Weight of a sheet letter	5	5	g	I
Total weight of used papers	**1.90E+06**	**9.50E+02**	**Ton**	**J=I*D/1e6**
CO2 reduction ratio (GC/OPC)		**2000**	**Ton/year**	J(GC)/J(OPC)

From this place, it is time to rethink again about changing our calendar system to a more efficient, user-friendly, easier to memorize, eco-friendly, and sustainable calendar system using one of the proposed OPC systems in this paper. The massive production of calendars every year is energy-consuming and material-consuming. Thus, the carbon footprint of the Gregorian calendar is high and should be reduced by any means.

5. CONCLUSION

The Gregorian calendar has been used for several centuries, in which it was introduced to correct the Julian calendar. Despite the success of the Gregorian calendar worldwide, and despite its accuracy, it is not easy to deal with the dates and days; hence sophisticated software is needed to calculate the dates of corresponding days. Billions of hard copies of the calendar are printed every year to help people organize better their life. Thus, millions of trees are cut every year to produce calendars and planners, which increases pollution and the emission of CO2. To minimize pollution and to go a further step toward a more sustainable society, this paper proposes an original perennial calendar system that is user- and eco-friendly. The proposed calendar system is very easy to interpret and memorize. Thus, there is no need to print hard copies of the calendar; therefore, millions of trees can be saved every year, and less pollution is emitted. For instance, we found that by using the Gregorian calendar system, the wasted energy used to check the dates and days on the calendar is almost 293 GWh/year. In addition, the CO2 emission and waste by producing paper-based calendars are 3.8 and 1.9 million tons per year, respectively, which are considered non-negligible numbers. From this place, the proposed calendar system uses optimization algorithms and mathematical modeling in order to obtain the optimal distribution of days, weeks, and months in a year. This paper compared the proposed calendar system with the Gregorian calendar and the International Fixed Calendar. Results show that the proposed one has more advantages compared to the other calendars, in which it reduces the energy demand and carbon footprint by 200 and 2000 times, respectively, compared to the Gregorian calendar. Further statistical analysis is required to see how people react regarding the idea of changing the calendar system and what will be the next step to do in order to implement it.

REFERENCES

[1] M. Grant, "Roman religion," in *Encyclopædia Britannica*, ed. England: Encyclopædia Britannica, inc., 2016.

[2] J. Rüpke, *The Roman calendar from Numa to Constantine: time, history, and the fasti*. John Wiley & Sons, 2011.

[3] A. K. Michels, *Calendar of the Roman Republic*. Princeton University Press, 2015.

[4] V. Emelianov, "Cultic Calendar and Psychology of Time: Elements of Common Semantics in Explanatory and Astrological Texts of Ancient Mesopotamia," *Comparative Mythology,* vol. 5, pp. 13-32, 2019.

[5] G. A. Barton, "Recent researches in the Sumerian calendar," *Journal of the American Oriental Society,* pp. 1-9, 1913.

[6] L. Brack-Bernsen, "The Observational Foundations of Babylonian Astronomy," in *Hellenistic Astronomy*: Brill, 2020, pp. 171-189.

[7] M. Boyce, "Further on the calendar of Zoroastrian feasts," *Iran,* vol. 43, no. 1, pp. 1-38, 2005.

[8] A. Dieckhoff, "Hebrew, the language of national daily life," in *Language, nation and state: Identity politics in a multilingual age*: Springer, 2004, pp. 187-199.

[9] M. Blomberg and G. Henriksson, "Literary and archaeoastronomical evidence for the origins of the Hellenic calendar in the Aegean Bronze Age," *BAR INTERNATIONAL SERIES,* vol. 1154, pp. 53-70, 2003.

[10] M. Dimitrijevic, E. T. Theodossiou, and P. Mantarakis, "Milutin Milankovic and the reform of the Julian Calendar in 1923," *Journal of Astronomical History and Heritage,* vol. 11, pp. 50-54, 2008.

[11] E. L. Cohen, "Adoption and reform of the Gregorian calendar," *Math Horizons,* vol. 7, no. 3, pp. 5-11, 2000.

[12] S. Joshi and U. Muley, "GREGORIAN CALENDAR," *Bulletin of the Marathwada Mathematical Society,* vol. 12, no. 1, pp. 65-75, 2011.

[13] H. H. Green, "Zenith Sun as the Means for Achieving Concordance Between the tonalpohualli and the Tropical Year Without Intercalation of Leap Days."

[14] M. B. Cotsworth, *The Rational Almanac: Tracing the Evolution of Modern Almanacs from Ancient Ideas of Time, and Suggesting Improvements, with Years, Half-years and Quarters Equated; 13 Months to the Year; Holidays and Festivals, Also Week Days Fixed on Permanent Dates to Gain Much More Public Convenience; 180 Illustrations Explaining the Mystery of the Pyramids, Sphinx, Obelisks, Druidical Circles, Mounds, Vertical Stones, Etc., Erected to Record Yearly Almanac Times*. Author, 1905.

[15] M. B. Cotsworth, "Proceedings and Transactions of the Royal Society of Canada, Third Series," 1908, vol. 2:

Royal Society of Canada, 1908, pp. 211-241. [Online]. Available: https://ia802608.us.archive.org/3/items/proceedingstrans32roya/proceedingstrans32roya.pdf. [Online]. Available: https://ia802608.us.archive.org/3/items/proceedingstrans32roya/proceedingstrans32roya.pdf

[16] J. K. SA Olaleru, FI Elegbeleye, TE Aniyikaiye, "Green Technology Solution to Global Climate Change Mitigation," *Energy, Environment, and Storage Journal*, vol. 1, no. 1, pp. 26-41, 2021. [Online]. Available: https://www.enenstrg.com/presentation/admin_pre_files/2110101244PDFX4OFJ3JXO0.pdf.

[17] N. A. Furkan Demirbas, "Evaluation of Carbon Footprint in a Waste Recovery/Recycle Facility," *Energy, Environment, and Storage Journal*, vol. 1, no. 1, pp. 7-12, 2021, doi: https://doi.org/10.52924/YANA8929.

[18] M. R. A. Saliha Ozarslan, Mustafa Kaya, Sebahattin Ünalan, "Evaluation of Tea Factory Wastes in Energy and Other Areas - A Review," *Energy, Environment, and Storage Journal*, vol. 1, no. 2, pp. 35-44, 2021, doi: https://doi.org/10.52924/QMDG6303.

[19] S. O. A. Rumeysa Ozden, Bilge Albayrak Çeper, Nafiz Kahraman, "The Relationship Between CO2 Emissions and Economic Growth in Turkey," *Energy, Environment, and Storage Journal*, vol. 1, no. 2, pp. 17-23, 2021, doi: https://doi.org/10.52924/WOSD3037.

[20] C. Mele. "Paper Calendars Endure Despite the Digital Age." The New York Times. https://www.nytimes.com/2016/12/29/business/paper-calendars.html (accessed November 04, , 2021).

[21] A. C. Dias and L. Arroja, "Comparison of methodologies for estimating the carbon footprint – case study of office paper," *Journal of Cleaner Production*, vol. 24, pp. 30-35, 2012/03/01/ 2012, doi: https://doi.org/10.1016/j.jclepro.2011.11.005.

[22] "70% Of Adults Rely on Digital Calendar." ECAL. https://ecal.com/70-percent-of-adults-rely-on-digital-calendar/ (accessed November 5, 2021).

[23] EUdesign. "Days in Each Month." EUdesign. http://www.eudesign.com/mnems/dayspcm.htm (accessed November 4, , 2021).

[24] L. Carroll, "To find the day of the week for any given date," *Nature*, vol. 35, no. 909, p. 517, 1887.

[25] B. E. Schwerdtfeger, "GAUSS'CALENDAR FORMULA FOR THE DAY OF THE WEEK," 2001.

[26] N. Dershowitz and E. M. Reingold, "Calendrical calculations," *Software: Practice and Experience*, vol. 20, no. 9, pp. 899-928, 1990.

[27] "One million calendars 'wrong due to bank holiday change'." BBC. https://www.bbc.com/news/uk-england-wiltshire-48661884 (accessed June 6, , 2020).

[28] Data-Reportal. "Digital Around the World." Data Reportal (KEPIOS PTE. LTD.). https://datareportal.com/global-digital-overview (accessed September 30, 2021).

[29] SCMO. "How Many Computers Are There In The World?" SCMO. https://www.scmo.net/faq/2019/8/9/how-many-compaters-is-there-in-the-world (accessed September 30, 2021).

[30] Northwestern-University. "Power Management Statistics." Information Technology Northwestern University. https://www.it.northwestern.edu/hardware/eco/stats.html (accessed September 30, 2021).

Research Article *Energy, Environment and Storage* (2021) 02-01:34-40

Energy, Environment and Storage

Journal Homepage: www.enenstrg.com

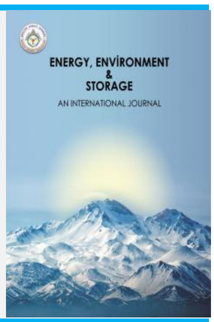

CFD MODELLING OF VOLTACAR ELECTRIC VEHICLE BODY FOR THE MOST EFFICIENT DRIVING CONDITIONS

Yakup Ogun SUZEN[1,4,5*], Emre OZDOGAN[2,4,5], Ibrahim SAN [3,4], Batuhan GURBUZ[2,4] Mehmet KACAR[3,4] Nesrin DEMİR[2,4,5] and Mehmet Fatih KAYA[*,2,4,5,6]

[1]Department of Mechanical Engineering, Faculty of Engineering, Erciyes University, 38039, Kayseri, Turkey

[2]Department of Energy Systems Engineering, Faculty of Engineering, Erciyes University, 38039, Kayseri, Turkey

[3]Department of Mechatronic Engineering, Faculty of Engineering, Erciyes University, 38039, Kayseri, Turkey

[4]Erciyes University VoltaCAR Electromobile & Hydromobile Team, 38039, Kayseri, Turkey

[5]Erciyes University H2FC Hydrogen Energy Research Group, 38039, Kayseri, Turkey

[6]BATARYASAN Enerji ve San.Tic. Ltd.Şti, Yıldırım Beyazıt Mah., Aşık Veysel Bul., ERÜ TGB İdare ve Kuluçka 4, No: 67/3/11, Melikgazi, Kayseri, Turkey

**Mehmet Fatih KAYA, ORCID: 0000-0002-2444-0583*

Nesrin DEMİR, ORCID: 0000-0001-8863-8911

ABSTRACT: In recent years, fossil fuels prices, greenhouse gas emissions, and need for sustainable energy sources have been increasing day by day. Thus, electric vehicles are seen as a promising candidate in the market due to their low-costs and cleaner fuel options such as electricity, hydrogen etc. Moreover, aerodynamics is one of the most important criteria to consider while designing an automobile for the most efficient driving conditions. For this reason, vehicle developers are studying to reduce drag resistance of the body to improve driving efficiency. On the other hand, Computational Fluid Dynamics (CFD) is one of the main tools for the automotive industry to obtain low-cost results before prototyping of any product. In this study, the aerodynamic characteristics of VoltaCAR electric vehicle is numerically investigated to obtain the best driving velocity. This car participates the TUBITAK-Electromobile car competition every year to achieve low fuel consumption for one hour driving. Thus, it is aimed that to minimize the resistance of the air hitting from the front, side, and roof of the vehicle. In the numerical model, polyhedral mesh structure is preferred to obtain faster convergence with fewer iterations, and shorter computation time is obtained compared to the tetrahedral mesh method. The aerodynamic drag coefficient (C_d) of the car model was calculated as approximately 0.17 at 22.22 and 27.78 m/s. The optimum velocity values were selected as 22.22 and 27.78 m/s by means of their lower C_d.

Keywords: Aerodynamics, Fuel-Efficiency, Drag Coefficient, Computational Fluid Dynamics, Electromobile, Polyhedral Mesh

Article History: Received:05.11.21; Revised: 15.11.2021; Accepted:26.11.2021; Availableonline: 26.11.2021
Doi: https://doi.org/ 10.52924/DGHR8227

1. INTRODUCTION

Energy consumption in developed and developing countries continues to increase day by day. Thus, energy demand will reach unsustainable levels in the future [1]. Today, the automotive industry is faced with challenges such as reducing emissions of exhaust gases into the atmosphere, increasing safe driving, and reducing the use of fossil-based fuels required for energy production. Therefore, use of hybrid and electric vehicles, biofueled cars and reducing engine sizes are very important for the sustainable transportation [2]. The development of electric cars has increased in response to the reality that future oil sources will be depleted. Since the last decade, electric vehicles have attracted a lot of attention as one of the potential solutions to reduce greenhouse gas emissions. About half of the total fuel energy is lost to come through the aerodynamic forces [3]. In a medium-sized car, the total resistance at 100 km/h is over 65% due to aerodynamics forces [4]. For this reason, vehicle developers are researching to reduce drag resistance. It also improves passenger comfort by providing ventilation, air conditioning, reducing mud formation on the vehicle, and reducing noise levels [5]. The aerodynamic development of the vehicle history has been gathered under two main headings. Firstly, it is focused on the wind

*Corresponding author: kayamehmetfatih@erciyes.edu.tr

that is hitting from the front of the vehicle (projectile area) at high speeds. Secondly, it is aimed to reduce the accumulation of mud or dirt on the windows and lights of the vehicles by arranging them according to the wing designs of the aircraft with an aerodynamic body [6]. CFD is a beneficial tools of fluid mechanics that uses numerical methods and algorithms to solve and analyze problems involving fluid flows. CFD is one of the vital processes for the automotive industry [7, 8]. Thus, it is important for the efficient driving conditions for the electric cars as well. In the future, internal combustion engines will be replaced by electric vehicles, fuel cell vehicles, and hybrid vehicles. Limited driving range is one of the challenge due to battery developments of electrical vehicles [9, 10]. In Turkey, there are few competitions organized by TEKNOFEST and TUBITAK Efficiency Challenge is a college-level student design competition in which students from colleges around the country to design and compete with racetracks each year. In this study, CFD analysis of the vehicle is conducted for a full-scale car model to obtain most efficient numerical outputs for the low fuel consumption driving. The purpose of this study is to produce low C_d car and optimize the car velocity range during the one hour driving time.

2. MODEL DEFINITION AND NUMERICAL SOLUTION METHOD

2.1 Physical Model

Geometry of the model car was created with SolidWorks design software. Rendering of the model was performed in SolidWorks Visualize tool. In the design process, it is aimed to obtain a low C_d, so that the dimensions are suitable to the rules and there are no sharp edges on the vehicle body [11]. Figure 1 shows the side view and the isometric view of the vehicle model.

(a)

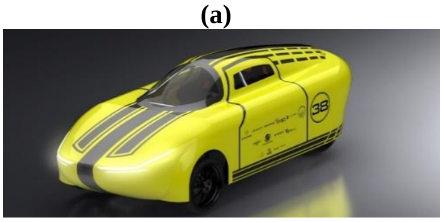

(b)

Figure 1. (a) Side view and **(b)** Isometric view of car model.

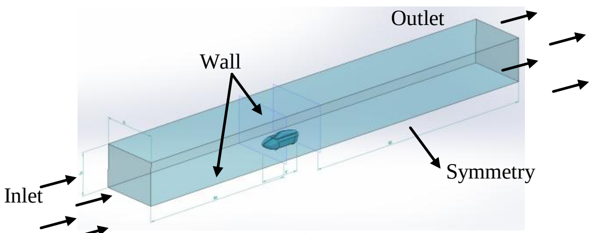

(a)

Figure 2. (a) Flow domain design and boundary regions.

In Figure 2 the flow domain and boundary conditions can be seen.

As given in Figure 2 the flow domain was created around the car in the SpaceClaim to perform the analysis. Length of the vehicle is x, then the distance from starting of the virtual box to the front end of the car is 5x whereas from the rear end of the car to the end of the virtual box is 10x [12, 13].

2.2 Mesh Generation

In Figure 3, the mesh structures of the model which is generated by ANSYS Fluent can be seen. Polyhedral meshes are preferred due to their advantages such as faster convergence with fewer iterations, the accuracy of wall shear stresses, and shorter computation time compared to the tetrahedral mesh method.

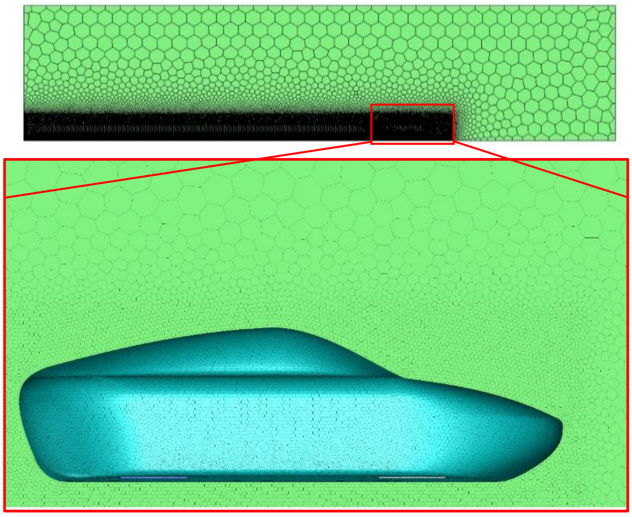

(a)

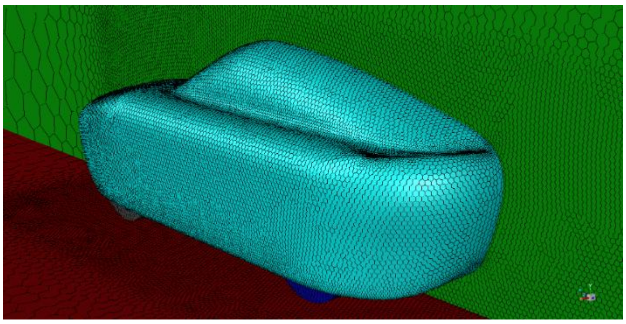

(b)

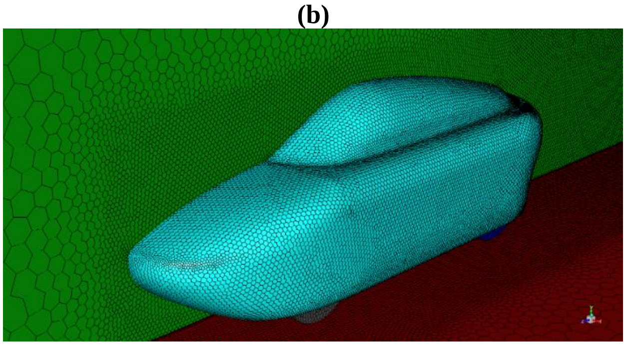

(c)

Figure 3. (a) Detailed view **(b)** Rear Isometric view **(c)** Front Isometric view of polyhedral meshing

The inlet flow is assumed as isothermal and incompressible, and the velocity of the air is set to 27.78, 22.22, and 16.67 m/s, respectively. The velocity values for the vehicle aerodynamics were performed according to the competition time as given in the rules completing for one hour. Therefore, according to racing track length, velocity was selected as the range of 16.67, 22.22 and 27.78 m/s. Also, the car body, ground plane, and wheels are defined as no-slip wall. At the outlet, the boundary condition is selected as a pressure outlet with a gauge pressure of 0 Pa [14-16]. There are approximately 2984497 polyhedral cell and 4459322 nodes in the model. In Figure 4, inlet and outlet region of the mesh structure can be seen.

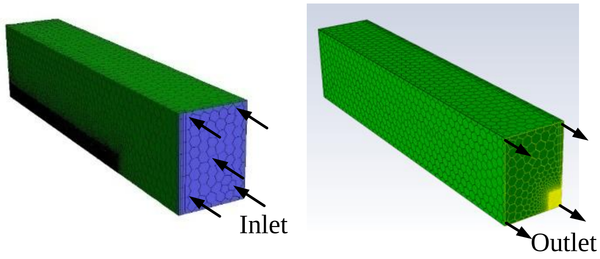

(a) (b)

Figure 4. (a) Inlet area, **(b)** outlet area for meshing

2.3. Mathematical Model

Laminar and turbulent flow are the two different forms of the flow. Laminar flow is defined as fluid particles are moving parallel to each other at a constant speed and without or smaller mixing condition with each other. On the other hand, turbulent flow is a kind of fluid motion that is described by chaotic changes in flow velocity and pressure [17-19].

Thus, the flow around the vehicle body can be defined by Navier-Stokes equation as given Eq.1 [20]:

$$\rho\left(\frac{\partial u_i}{\partial t}+u_j\frac{\partial u_i}{\partial x_j}\right) = -\frac{\partial P}{\partial x_i}+\mu\frac{\partial^2 u_i}{\partial x_j \partial x_j}+f_i \qquad (1)$$

Where u represents the velocity, t is the time, x is the position, P is the pressure, and ρ is density in kg/m^3. In the numerical model, k – ε turbulent model is used and transport equations for standard k – ε turbulent model can be written as Eq. 2:

$$\frac{\partial}{\partial t}(\rho k)+\frac{\partial}{\partial x_i}(\rho k u_i)=\frac{\partial}{\partial x_j}\left[\left(\mu+\frac{\mu_t}{\sigma_k}\right)\frac{\partial k}{\partial x_j}\right]+G_b+G_k-\rho\,\varepsilon-Y_m+S_k \qquad (2)$$

In these equations, G_b is the generation of turbulence kinetic energy due to buoyancy, G_k represent the generation of turbulence kinetic energy due to the mean velocity gradients, Y_m describes the contribution of the fluctuating dilatation incompressible turbulence to the overall dissipation rate. C_{1e}, C_{2e} and C_{3e} are constants. σ_k and σ_ε are the turbulent Prandtl numbers for k and ε, respectively. S_k and S_e are user-defined source terms. C_f is the skin-friction coefficient.

To model dissipation (ε) Eq.3 can be used:

$$\frac{\partial}{\partial t}(\rho\varepsilon)+\frac{\partial}{\partial x_i}(\rho\varepsilon u_i)=\frac{\partial}{\partial x_j}\left[\left(\mu+\frac{\mu_t}{\sigma_\varepsilon}\right)\frac{\partial\varepsilon}{\partial x_j}\right]+C_{1\varepsilon}\frac{\varepsilon}{k}(G_k+C_{3\varepsilon}G_b)-C_{2\varepsilon}\rho\frac{\varepsilon^2}{k}+S_\varepsilon \qquad (3)$$

To model shear stress (τ_w) on the wall Eq.4 can be used [21]:

$$\tau_w=\frac{C_f\rho U_{freestream}^2}{2} \qquad (4)$$

Conservation of mass, momentum, and energy are fundamental equations for CFD calculations [22]. Eq.5 can be used to calculate Reynolds number as below:

$$Re=\frac{\rho VL}{\mu} \qquad (5)$$

In this equation, V represents velocity of the fluid in m/s, μ describes dynamic coefficient of viscosity in N.s/m^2, and L is the characteristic length in m. Reynolds number is a dimensionless number that can be used to describe the flow of fluid[23].

Aerodynamic drag force (F_d) causes more resistance force in passenger automobiles at higher speeds. It is a resistive force that affects the performance of a vehicle. Also, this component of resistance might become overpowering at high speeds [24]. Thus, vehicle developers have challenge to reduce drag resistance. In Figure 5, F_d and lift force (F_L) regions can be seen.

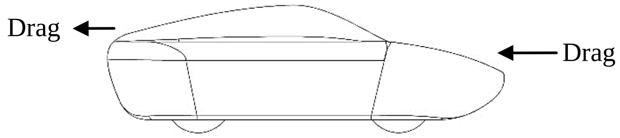

Figure 5. F_d and F_L on the vehicle body.

F_d is known as the force parallel to the flow direction. The drag coefficient (C_d), which is a dimensionless number, is given as Eq.6 below:

$$C_d=\frac{2F_d}{\rho V^2 A} \qquad (6)$$

Where F_d is drag force in N, ρ is density in kg/m^3, V is velocity in m/s, and A is the refence area in m^2. Reference area of the model can be seen as given in Figure 6.

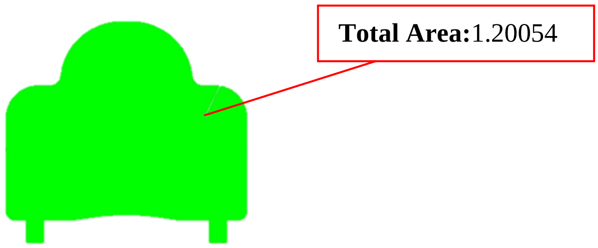

Figure 6. Reference area

The C_d of the vehicles are approximately 1.0 for large semi-trailers, 0.4 for minivans, and 0.3 for passenger cars [25]. The component of the aerodynamic force perpendicular to the direction of flow is defined as the F_L. F_L is very important to ensure the controllability of the vehicles and as the speed increases. The lift coefficient (C_L) is a dimensionless coefficient that relates the lift created by a lifting body to the fluid density over the body, the fluid velocity, and a reference area can be calculated by Equation (7).

$$C_L=\frac{F_l}{\frac{1}{2}\rho V^2 A} \qquad (7)$$

In Table 1, the solution parameters for the Ansys model can be seen.

Table 1. Fluent solver parameters

Solver		Fluent		
Formulation		Implicit		
Time		Steady		
Temperature (K)		288.16		
Velocity (m/s)		16.67	22.22	27.78
Area (m^2)		0.60027 (Symmetry)		
Velocity Formulation		Absolute		
Gauge Pressure (Pascal)		0		
Turbulence Models		SST-k- ε Realizable-Enhanced Wall Treatment		
		SST–k-ω		
Scaled Residuals		10^{-4}		
Fluid Properties	**Fluid Type**	Air		
	Density	ρ = 1.225 (kg/m³)		
	Viscosity (kg/m-s)	1.7894e-05		

3. RESULTS AND DISCUSSION

CFD-Post software is used to determine streamlines, pressure, velocity distributions, velocity vectors, C_d, and pressure results. In Figure 7, streamlines and velocity display can be seen around the vehicle body.

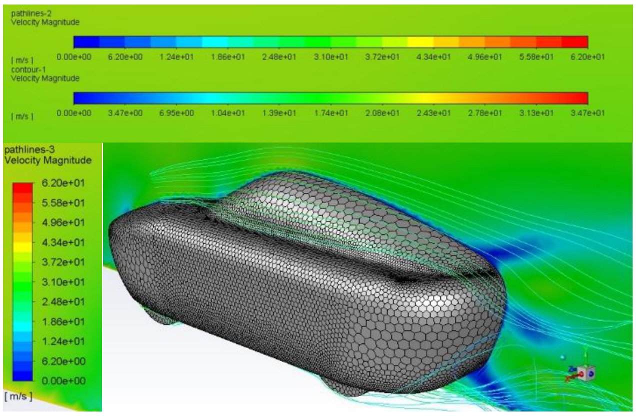

Figure 7. Streamlines and velocity display

To understand the flow around the model, a flow visualization test was performed in the Ansys Post-processing .The flow analysis on the vehicle is performed on three different inlet velocity such as 16.67, 22.22, 27.78 m/s to get the results for the C_d, and C_L.

For 16.67 m/s inlet velocity, it has been observed that the F_d of the vehicle decreases with the C_d and C_L, respectively. C_d, and C_L are became stable after 100 iterations and the residual graph is converged. C_d and C_L are calculated as 0.1818, and 0.09531, respectively. In Figure 8, at 16.67 m/s, pressure, turbulent kinetic energy, velocity magnitude, and wall shear stress can be seen.

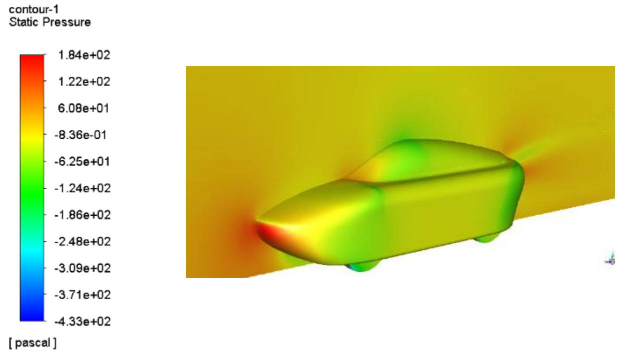

(a)

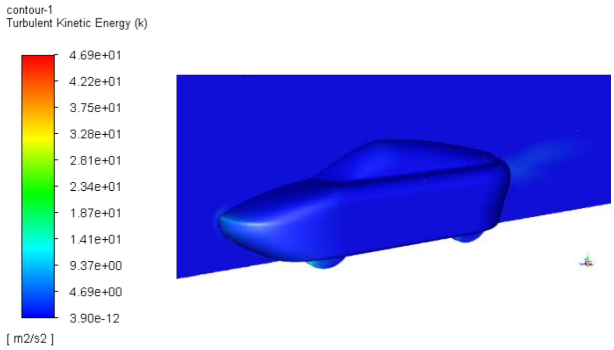

(b)

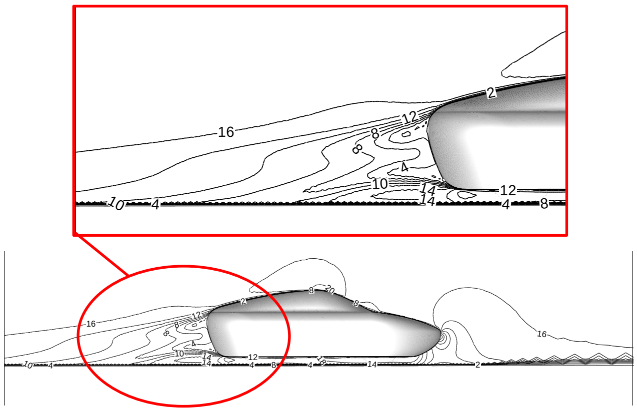

(c)

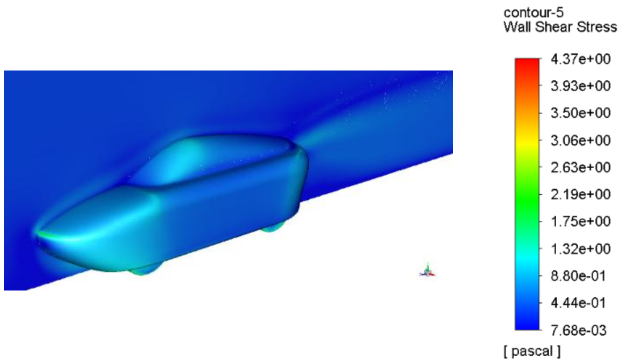

(d)

Figure 8. (a) Pressure, **(b)** Turbulent Kinetic Energy , **(c)** Velocity Magnitude, and **(d)** Wall Shear Stress figures at 16.67 m/s

Figure 8. (a) shows the pressure contours over the vehicle body and the maximum pressure occurs front surface of the car. The minimum pressure value occurs in the

separated flow region. This is due to the fluid's velocity being close to zero in these regions. Pressure values at low speeds, relatively lower than at higher speeds. According to the pressure distribution on the symmetric surface, the maximum and minimum pressures are calculated as 153 Pa and -93 Pa, respectively. Figure 8. (b) shows the contour of turbulence kinetic energy on the symmetry plane. Figure 8. (c) represent the velocity streamlines in the symmetry plane. Figure 8. (d) shows the wall shear stress distribution in the body. The stress values are small which is around 0.2- 2 Pa in the vehicle body. Separated airflows may occur in the shear stress which are close to 0 point like wheel and underbody of the vehicle. The vortex under the vehicle not only increases the aerodynamic drag but also increases the pressure drag by changing the flow area behind the vehicle.[26]

C_d, and C_L are became stable after 125 iterations and the residual graph is converged. C_d and C_L are calculated as 0.1801, and 0.0939, respectively. These C_L and C_d values show better aerodynamics characteristics when the car move faster. In Figure 9 shows the pressure, velocity, turbulent kinetic energy and wall shear stress distrubution of the vehicle body at 22.22 m/s.

Figure 9. (a), and (c) shows the pressure contour and velocity magnitude all over the vehicle body. According to the pressure distribution on the symmetric surface, the maximum and minimum pressures are calculated as 270 Pa and -180 Pa, respectively. As shown in Figure 9. (a) pressure values are increased by velocity increment. The maximum value of turbulence kinetic energy was found in the vehicle's rear section. As seen in the Figure 9. (d) wall shear stresses increase with respect to speed especially on the front panel and rear side of the car body.

The C_d and C_L are calculated as 0.1788 and 0.0926 respectively. C_L is decreased from 0.0939 to 0.0926. In Figure 10 shows the static pressure, turbulent kinetic energy, velocity and wall shear stress can be seen. As shown in Figure 9. (a) pressure values increase due to velocity increment. The maximum and minimum pressures are calculated as 300 Pa and -240 Pa, respectively, As seen in the Figure 9, wall shear stresses on the rear side of the vehicle is close to 0 which may occur separated airflows with respect to the turbulence. The stress values are small which is around 1.2- 4 Pa in the vehicle body. The results of the C_d and C_L at different speeds and turbulence models can be seen in Table 2.

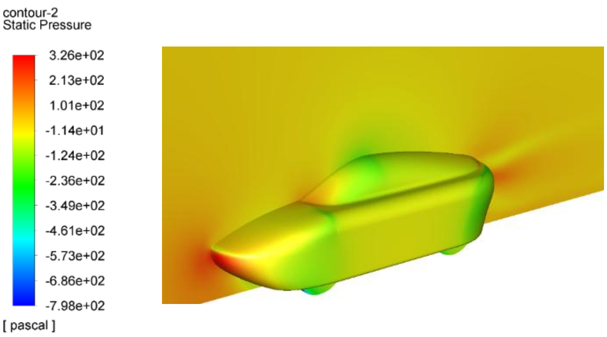

(a)

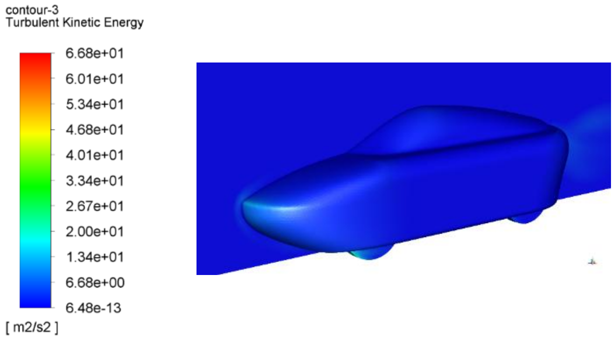

(b)

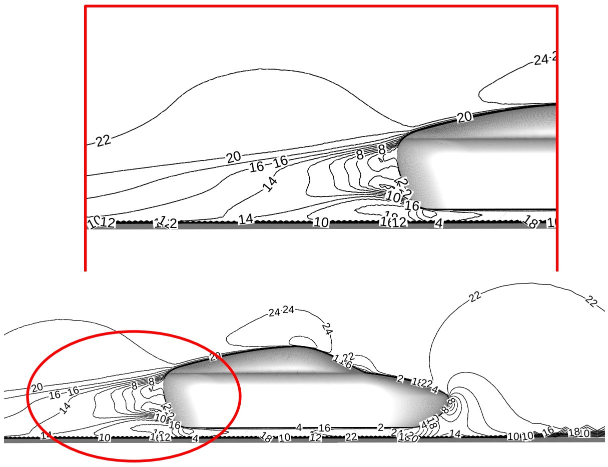

(c)

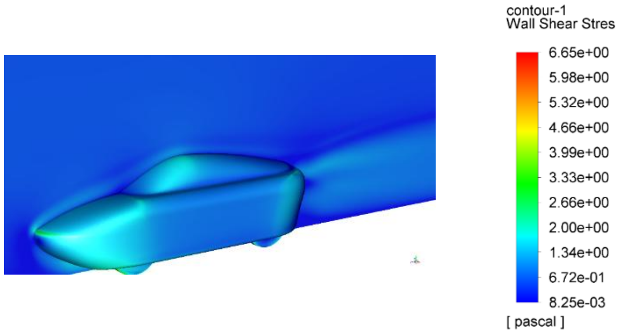

(d)

Figure 9. (a) Pressure, **(b)** Turbulent Kinetic Energy , **(c)** Velocity Magnitude, and **(d)** Wall Shear Stress figures at 22.22 m/s

Table 2: C_d and C_L Results in turbulence model SST-k- ε Realizable – Enchanced Wall Treatment and SST-k-ω

RESULTS		Velocity (m/s)		
		16.67	**22.22**	**27.78**
SST-k- ε Realizable-Enhanced Wall Treatment	C_d	0.1833	0.1823	0.1636
	C_L	0.1684	0.1674	0.1140
SST–k-ω	C_d	0.1818	0.1801	0.1788
	C_L	0.09531	0.0939	0.0926

As seen in the Table, in the higher speed, F_d increases. This increment occurs at the front of the vehicle. As can be seen from the table, C_d in terms of fuel consumption at 22.22 - 27.78 m/s shows more efficient driving. On the other hand, the air inlet from under the vehicle exerts pressure to lift the vehicle up, so in case of any bending, the vehicle may be easily skidded, and it may cause rolling over during the road driving. For this reason, automotive developers are tried to increase the downforce by giving curvature to the infrastructure of the cars. As given in Table 2, the C_L value for this vehicle is calculated as between 0.00201 and 0.00719. The results were compared with another turbulence model, SST k-ω, and it was found that there is no any significant difference between the results**.**

Figure 10 (a), and (c) shows the pressure contour and velocity magnitude all over the vehicle body. According to the pressure distribution on the symmetric surface, the maximum and minimum pressures are calculated as 270 Pa and -180 Pa, respectively. As shown in Figure 10 (a) pressure values increase due to velocity increment. The maximum value of turbulence kinetic energy was found in the vehicle's rear section. As seen in the Figure 10 (d) wall shear stresses increase with respect to speed especially on the front panel and rear side. In higher speed values, F_d value is increased. The aerodynamic F_d on the vehicle are dominant at 22.22 -27.78 m/s speeds, which is an important place in flow analysis. Therefore, the F_d and aerodynamic frictions in the vehicle is important parameter for fuel consumption which is desired to reduce pressure on the front vehicle. F_d on the car is around 40-60 N at 22.22 and 27.78 m/s. It has been observed that due to the turbulence regions formed at high speeds the graph is more difficult to converge than at low speed.

The C_d have closer results compared to the F_d. It can be also observed that the same situation caused by the turbulence zone is obtained in C_d results. When C_d value of the vehicle has increased, fuel consumption increases, also performance losses occur. As a result, C_d is computed approximately 0.17 at 22.22 – 27.78 m/s. For this reason, the C_d has an important place for automotive industry.

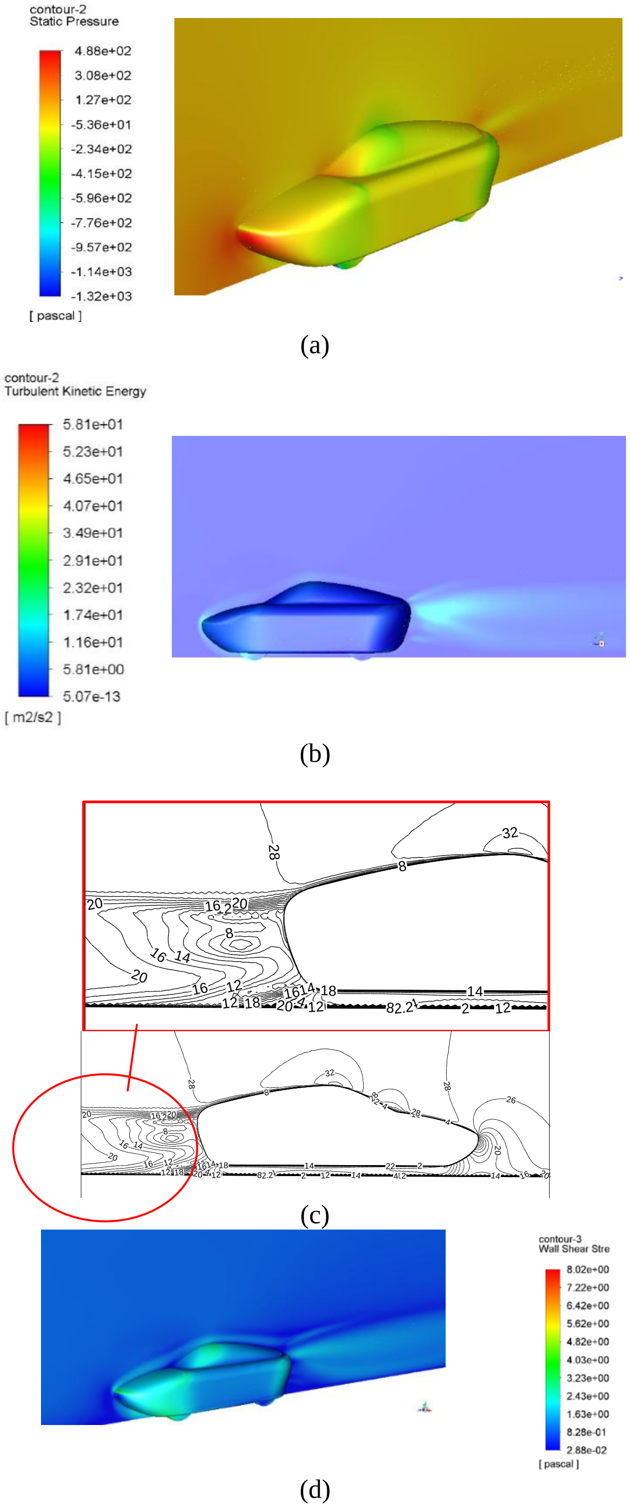

Figure 10. (a) Pressure, **(b)** Turbulent Kinetic Energy , **(c)** Velocity Magnitude, and **(d)** Wall Shear Stress figures at 27.78 m/s

4. CONCLUSION

The aerodynamic characteristics of the body shape of the VoltaCAR, which was produced to participate in the TUBITAK Efficiency Challenge race, is realized in 3D numerical model using ANSYS Fluent software. This vehicle design was conducted according to the race rules. For numerical modeling, the mesh method was preferred as polyhedral, thus shortening the solution time and faster converge for the solution. The static pressure is calculated approximately as 270 Pa on the front side of the vehicle and between 67-120Pa on the vehicle body at 22.22 m/s. Also, the static pressure which is on the front side of the vehicle has increased approximately 400Pa, and in the vehicle body, it is between 55 and 150 Pa at 27.78 m/s. The pressure created by the air affects the front of the vehicle. It is distributed to the lower and upper sides along with the slope in the vehicle design, thus allowing the wind to flow more smoothly, thereby reducing the pressure. Depend on the speed, there is 50% much more static pressure is obtained on the front of the vehicle, but this increase is lower than the vehicle body. Thanks to these results, the pressure increase of the vehicle body is minimized. On the other hand, Cd of the car model is calculated as around 0.17 at 22.22 and 27.78 m/s. As a conclusion when increasing the speed, the Cd decreases, but the Fd and pressures at the side of the vehicle increase. Passenger vehicles have an average C_d of 0.25, the C_d computed for this vehicle design is much lower depending on its speed. As a result, the most efficient fuel consumption range for this vehicle was determined between 22.22 and 27.78 m/s. For the race conditions, these parameters can be further improved by optimizing critical points of the flow with aerodynamics experimental studies.

Acknowledgements

Authors would like to thank TÜBİTAK Efficiency Challenge Organization Committee and all Enerjist-VoltaCAR Electric and Hydrogen Fuel Cell car project team members for their great effort on the car design and production successfully.

REFERENCES

[1] Michaelides EES. (2012). Alternative energy sources: Springer Science & Business Media..

[2] Davila A, Aramburu E, Freixas A. (2013). Making the best out of aerodynamics: Platoons. SAE Technical Paper.

[3] Hassan SR, Islam T, Ali M, Islam MQ. (2014). Numerical study on aerodynamic drag reduction of racing cars. Procedia Engineering. 90:308-13.

[4] Wood R. (2015). Reynolds number impact on commercial vehicle aerodynamics and performance. SAE International Journal of Commercial Vehicles.8:590-667.

[5] Sivaraj G, Parammasivam K, Suganya G. (2018). Reduction of aerodynamic drag force for reducing fuel consumption in road vehicle using basebleed. Journal of Applied Fluid Mechanics.11:1489-95.

[6] Sivaraj G, Parammasivam K, Prasath M, Vadivelu P, Lakshmanan D. (2021). Flow analysis of rear end body shape of the vehicle for better aerodynamic performance. Materials Today: Proceedings.

[7] Pal S, Kabir S, Talukder M. (2015). Aerodynamic analysis of a concept car model. Proceedings of the third ICMERE.26-9.

[8] Chandra S, Lee A, Gorrell S, Jensen CG. (2011). CFD analysis of pace formula-1 car. Computer-Aided Design & Applications, PACE (1):1-14.

[9] Nalanagula S, Varadharajan G. (2016). Aerodynamics drag reductions methodology for the commercial vehicles using computational fluid dynamics. SAE Technical Paper.

[10] Huluka AW, Kim C-H. (2021). A Numerical Analysis on Ducted Ahmed Model as a New Approach to Improve Aerodynamic Performance of Electric Vehicle. International Journal of Automotive Technology.22:291-9.

[11] Lanfrit M. (2005). Best practice guidelines for handling Automotive External Aerodynamics with FLUENT. Version.

[12] Kaluva ST, Pathak A, Ongel A. (2020). Aerodynamic drag analysis of autonomous electric vehicle platoons. Energies.13:4028.

[13] Watanabe K, Matsuno K. (2009). Moving computational domain method and its application to flow around a high-speed car passing through a hairpin curve. Journal of computational Science and Technology. 3:449-59.

[14] Spiegel M, Redel T, Zhang YJ, Struffert T, Hornegger J, Grossman RG, et al. (2011). Tetrahedral vs. polyhedral mesh size evaluation on flow velocity and wall shear stress for cerebral hemodynamic simulation. Computer methods in biomechanics and biomedical engineering. 14:9-22.

[15] Balafas G. (2014). Polyhedral mesh generation for CFD-analysis of complex structures. Diplomityö Münchenin teknillinen yliopisto.

[16] Kleber A. (2001). Simulation of airflow around an Opel Astra vehicle with Fluent. Journal Article, International Technical Development Center Adam Opel AG.

[17] Hoffman J, Johnson C. (2007). Laminar and Turbulent Flow. Computational Turbulent Incompressible Flow: Applied Mathematics: Body and Soul 4. 51-5.

[18] Vasamsetti S. Streamlining and Aerodynamic Performance Add-on Devices of Sports Cars.

[19] Batchelor CK, Batchelor G. (2000). An introduction to fluid dynamics: Cambridge university press.

[20] Hetawal S, Gophane M, Ajay B, Mukkamala Y. (2014). Aerodynamic study of formula SAE car. Procedia Engineering.97:1198-207.

[21] Thabet S, Thabit TH. (2018). CFD simulation of the air flow around a car model (Ahmed body). International Journal of Scientific and Research Publications. 8:517-25.

[22] Damjanović D, Kozak D, Živić M, Ivandić Ž, Baškarić T. (2011). CFD analysis of concept car in order to improve aerodynamics. Járműipari innováció. 1:108-15.

[23] Shi X, Sun DJ, Zhang Y, Xiong J, Zhao Z. (2020). Modeling emission flow pattern of a single cruising vehicle on urban streets with CFD simulation and wind tunnel validation. International Journal of Environmental Research and Public Health;17:4557.

[24] Mannering FL, Washburn SS. (2020). Principles of highway engineering and traffic analysis: John Wiley & Sons.

[25] Sofian M, Nurhayati R, Rexca A, Syariful SS, Aslam A. (2014). An evaluation of drag coefficient of wind turbine system installed on moving car. Applied Mechanics and Materials: Trans Tech Publ; p. 689-93.

[26] Yuan Z, Wang Y. (2017). Effect of underbody structure on aerodynamic drag and optimization. Journal of Measurements in Engineering. 5:194-204.

Founded in 2016, ourassociation is opentoeveryonewho is interested in energyanddevotedtosustainability.

ERCIYES ENERGY ASSOCIATION

2022